STUDY OF WELD QUALITY OF AISI 304L AUSTENITIC STAINLESS STEEL BY USING TIG WELDING

By

SUTONU ORAON

Examination Roll No. – M4MEC22005

Registration No. - 131722 of 2015-2016

Class Roll No.- 002011202005

Under the guidance of

Dr. NABENDU GHOSH

&

Prof. (Dr.) SUBHASH CHANDRA PANJA

Department of Mechanical Engineering

Jadavpur University

THESIS

SUBMITED IN PARTIAL FULFILMENT OF THE REQUIREMENTS FOR THE DEGREE OF

MASTER OF MECHANICAL ENGINEERING

IN THE FACULTY OF ENGINEERING AND TECHNOLOGY

JADAVPUR UNIVERSITY

DEPARTMENT OF MACHANICAL ENGINEERING

JADAVPUR UNIVERSITY

KOLKATA – 700032

2022

DECLARATION OF ORIGINALITY AND COMPLIANCE OF ACADEMIC ETHICS

I, Mr. Sutonu Oraon do hereby declare that this thesis entitled “Study of weld quality of AISI 304L Austenitic stainless steel by using TIG welding” contains literature survey and original research work done by the undersigned candidate as part of Master of Mechanical Engineering studies.

All information in this thesis have been obtained and presented in accordance with existing academic rules and ethical conduct. I declare that, as required by these rules and conduct, I have fully cited and referred all materials and results that are not original to this work.

I also declare that I have checked this thesis as per the “Policy on Anti Plagiarism, Jadavpur University”, and the level of similarity as checked by iThenticate software is 10 %.

Signature of Candidate:

Date:

JADAVPUR UNIVERSITY

Raja S.C. Mallick Road, Kolkata 700032, West Bengal, India

FACULTY OF ENGINEERING AND TECHNOLOGY

CERTIFICATE OF RECOMMENDATION

We hereby recommend that the thesis prepared under our supervision by Mr.Sutonu Oraon, examination roll number - **M4MEC22005** , entitled "**STUDY OF WELD QUALITY OF AISI 304 L AUSTENITIC STAINLESS STEEL BY USING TIG WELDING** " be accepted in partial fulfilment of the requirements for the Master of Mechanical Engineering.

To the best of our knowledge, the matter embodied in the thesis has not been submitted to any other University/Institute for the award of any degree or diploma.

THESIS SUPERVISOR	THESIS CO-SUPERVISOR
Dr. Nabendu Ghosh Assistant Professor, Department of Mechanical Engineering, Jadavpur University, Kolkata 700032, India	Prof. (Dr.) Subhash Chandra Panja Professor, Department of Mechanical Engineering, Jadavpur University, Kolkata 700032, India
Prof. (Dr.) Chandan Mazumdar Dean, Faculty Council of Engineering & Technology, Engineering, Jadavpur University, Kolkata 700032, India	Prof. (Dr.) Amit Karmakar Head of the department, Department of Mechanical Jadavpur University, Kolkata 700032, India

JADAVPUR UNIVERSITY

Raja S.C. Mallick Road, Kolkata 700032, West Bengal, India

FACULTY OF ENGINEERING AND TECHNOLOGY

CERTIFICATE OF APPROVAL

The foregoing thesis is hereby approved as a credible study of an engineering subject carried out and presented in a manner satisfactory to warrant its acceptance as a pre-requisite to the degree for which it has been submitted. It is understood that by this approval the undersigned do not endorse or approve any statement made, opinion expressed or conclusion drawn therein but approve the thesis only for the purpose for which it is submitted

_____

Committee

On Final examination _____

For evaluation of the thesis

_____

Signature (s) of the examiners

ACKNOWLEDGEMENT

The author gratefully expresses his sincere gratitude to the thesis supervisors **Prof. (Dr.) Subhash Chandra Panja** and **Dr.Nabendu Ghosh**, Mechanical Engineering Department, Jadavpur University, Kolkata for their invaluable guidance, suggestions and encouragement in the course of the present work.

The author is indebted to **Dr.Sanjib Acharya**, faculty members of Mechanical Engineering Department, Jadavpur University, for their invaluable help and advice to this thesis work from time to time. The author acknowledges the help rendered by **Dr. Goutam Nandi** and **Dr.Titas Nandi,** Superintendent, Blue Earth Machine Shop, Mechanical Engineering Department, Jadavpur University. The author is very much grateful to **Prof.SumantaNeogi**, Professor and Ex-Head, Mechanical Engineering Department, Jadavpur University and **Prof. Amit Karmakar,** Professor and Head, Mechanical Engineering Department, Jadavpur University for giving encouragement for completing the thesis.

The author feels that the thesis would not have been completed without the efforts rendered by staff members of FFDA Laboratory, Jadavpur University. The author is indebted to his friend at Mechanical Engineering Department of Jadavpur University. The author would like to convey thanks to **Shri Anshuman Roy**, Ph.D student of Power Engineering Department, for his constant support and help.

The author will fail in his duty if he does not offer thanks to all his friends, seniors and class-mates for presenting the thesis in the present form.

The author pays his sensible appreciation to all those who submitted the invaluable database of information in the internet and also to those who are maintaining such invaluable database records, providing a great help for the researchers in the field of science and technology.

SUTONU ORAON

ABSTRACT

Weld quality mainly depends on features of bead geometry, mechanical-metallurgical characteristics of the weld as well as on various aspects of weld chemistry and these features are expected to be greatly influenced by various variables such as welding geometry, groove angle, shielding type and mixture, and different input parameters: current, voltage, electrode stick-out, gas flow rate, edge preparation, position of welding, welding speed, nozzle to plate distance etc. Moreover, the cumulative effect of various input parameters determines the extent of joint strength that should meet the functional aspects of the weld in practical field of application. Therefore, preparation of a good quality weld seems to be a challenging job. In doing so, parametric optimization, analysis of weld pool solidification and heat transfer, metallographic characterization, development of ANN models, analysis of joint performance etc. become important. Extensive investigation relating to all these aspects will lead to create a strong knowledge-base which will help people in practical field to use TIG in a more predictable way, ensuring desired quality of weld. AISI 304L Austenitic stainless steels have been butt welded as per Taguchi designs of experiments. Several levels of current, gas flow rate and Arc gap have been used to do butt welding. Three levels of current, gas flow rate and Arc gap have been selected based on L9 Taguchi Orthogonal Array design of experiment. After welding, visual inspection of all the samples has been done. X-ray radiography tests are conducted next. Now tensile test specimens are made by machining the welded samples. During preparation of tensile test specimen, small cut-outs are made which have subsequently been ground, polished and finally etched to obtain samples for microstructural studies. Hardness of all the welded samples has been carried out. The results of these tests are discussed and interpreted. The observed data of the ultimate tensile strength, yield strength and percentage elongation under varied conditions of welding are analyzed by using Grey based Taguchi methodology.

CONTENTS

CHAPTER1

INTRODUCTION

1.1 INTRODUCTION

Welding is the technique of permanently uniting two metals, either similar or dissimilar, using heat and pressure, with or without the use of filler metal, to form a single piece. Compared to casting and riveting, this is a more cost-effective and speedier option. Today, welding is widely accepted as a very adaptable method of metal manufacturing around the world. With numerous well-established welding methods available, arc with coated electrodes is still the most widely used welding procedure in the world.

The electric dynamo, created in 1877, served as a precursor to arc welding. Auguste de Meritens, a French inventor, was the first to utilise electric arc welding to connect the various elements of storage battery plates in 1881. In 1800, the electric arc was first discovered, and arc welding began to take shape. Elihu H. Thompson discovered resistance welding in 1886, which was first employed. By using carbon electrode, N. V. Bernado established the first true arc welding, which is defined as the melting and fusing metal by the use of electrodes. In 1895, N.G. Slavianoff attempted to use a metallic electrode, but he had limited success because he used bare metal electrodes. This was made possible by the introduction of the flux coated electrode in 1905. Aluminum and magnesium were still difficult to weld in the early twentieth century because they reacted quickly with the air, creating a porous and dross-filled weld. When utilizing flux-coated electrodes, the weld area was not adequately protected from contaminants. To address the issue in the early 1930s, bottled inert gases were utilized. The aircraft industry used a direct current, gas-shielded welding technique for welding magnesium a few years later.

Welding processes that use helium as a shielding gas, including heliarc or tungsten inert gas welding, were developed in 1941. At first, the electrode quickly warmed, and despite the high melting point of tungsten, tungsten particles were transmitted to the weld. The polarity of the electrode was reversed from positive to negative in order to fix this issue, but this left the electrode unsuitable for welding many non-ferrous materials. Alternating current units have also made it possible to steady the arc and generate high-quality aluminium and magnesium welds.Using tungsten inert gas shielded arc welding, an electric arc is maintained between a nonconsumable tungsten electrode and the object being welded (TIG welding). As the TIG torch

heats up, an inert gas blanket is fed through to shield the molten metal, the electrodes, and the heat-affected zone (HAZ).

The quality of a TIG weld can be affected by a wide range of process control parameters. Our welds are made up of a wide range of chemical properties, as well as geometric features of the bead geometry, mechanical-metallurgical characteristics, and a variety of other factors. Because the process control parameters directly affect weld quality, this information must be known before selecting an appropriate process environment that can meet the needs of the desired weld quality.

Welding current and gas flow rate, as well as the influence of filler metal modification on mechanical and metallurgical properties of the weld, have been examined in this study. Parametric optimization has also been attempted. Data was analyzed and modelled using regression, ANOVA, and Taguchi-based grey relational methods.

1.2 WELDING AND ALLIED PROCESSES

With or without the use of pressure, welding is a process of fusing two metals together through fusion, whether or not the metals are similar or dissimilar. According to a wide range of authors, welding (and related) processes have been categorized in many ways. Classification of welding process is shown in figure 1.1

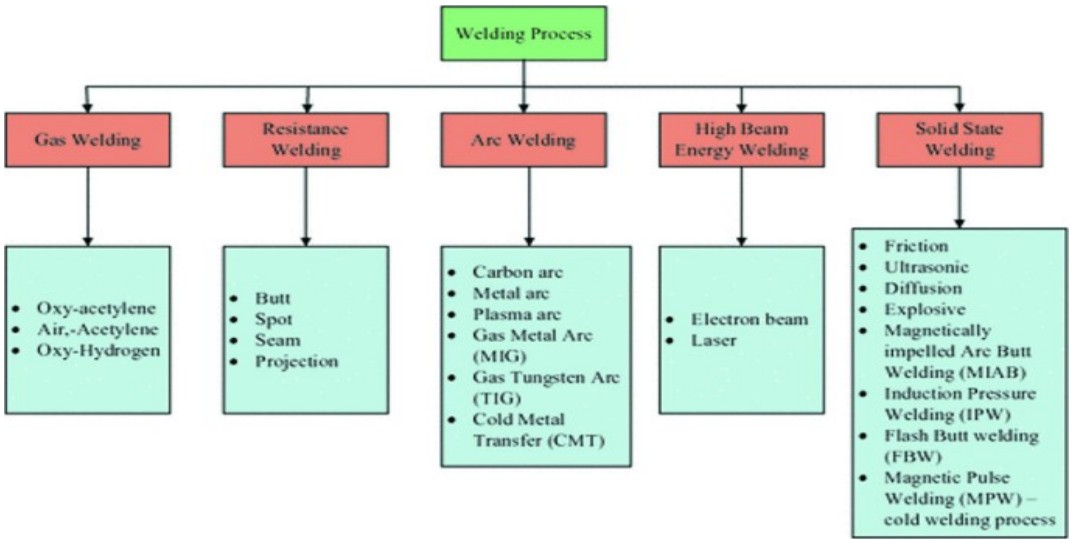

Figure 1.1 Classification of welding process

1.3 PRINCIPLE OF ARC WELDING

When two electrodes come into contact with each other, an arc is formed. Plasma is an electrically conducting heated ionized gas. Electric arcs for welding are known as "welding arcs," and they are often formed between a thin rod (and wire) and a plate. Generally, a welding arc operates at a voltage between 10 to 50 volts, which is a high current, low voltage discharge. Arcs are load resistors in welding circuits.

Arc welding, in general, is the result of the cathode emitting electrons into the ionised hot gas that fuse with the anode. In order to conduct an examination of the welding arc, the cathode spot, cathode space, arc column, anode space, and anode spot are often split into five separate zones. Figure 1.2 shows that the voltage drops across the cathode and anode drop zones are relatively sharp, whereas the voltage drops across the arc column are more gradual.

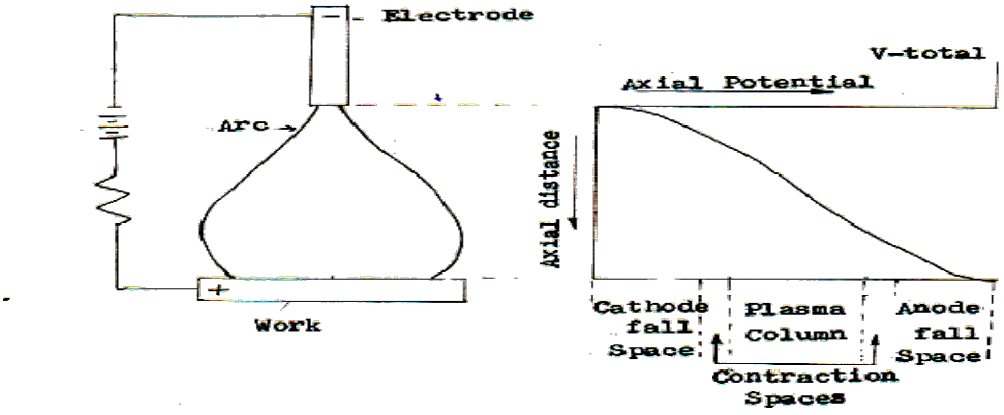

Figure 1.2 Shape of welding arc and potential drop across a welding arc

From the figure it is evident that the arc voltage (V) is a sum of cathode drop (V_c), column (V_p) and anode drop (V_a), it can then be expressed as,

$$V = V_c + V_p + V_a$$

In shielded metal arc welding and gas metal arc welding, the shape of the welding arc can vary greatly due to the fact that the rod electrode in these techniques is consumable. To truly understand a welding arc's behaviour, one must be familiar with the characteristics of each of the arc's zones.

There is an anode (the positive DC supply pole) and a cathode (the negative supply pole). ions flow from positive to negative poles in the presence of metal ions, which are positively charged and so drawn to the negative pole in the arc column's electrical theory

When the cathode and anode are first touched, an air gap is formed, and ions travel across this air gap due to the negative cathode's attraction. They're looking for a negative charge that will restore equilibrium to an atomic structure that has been damaged by electricity. A thermal ionization layer is created when ions collide with atmospheric gas molecules as they pass through this air gap. Because of its high-resistivity properties, the ionized gas column facilitates faster transfer of electrons from the anode to the cathode. As the ions hit the cathode, they generate heat. Heating can be explained using ionic theory. The arc column isn't totally explained by this. So the electron theory is needed to explain it more clearly. Figure 1.3 illustrates the concept of electrical theory.

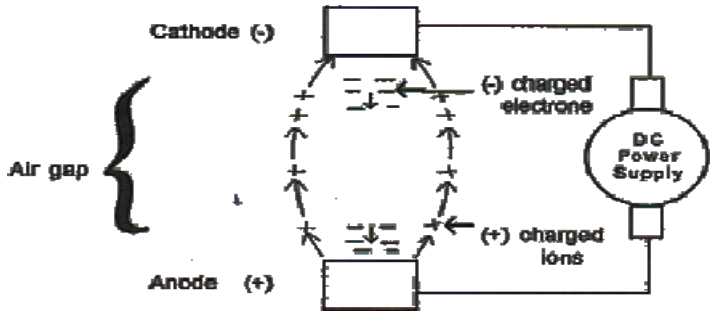

Figure 1.3 Electron theory of arc column. [60]

This generates an increase in current density, which results in the release of electrons from the cathode due to the thermoionic emission as the metallic bridge is broken. It is possible to calculate the rate at which electrons are released from the hot surface using the formula $I = C\theta 2 \exp(-\beta) / \theta$, where I is in amp/ cm2, θ is the absolute temperature, C is a constant and β is given by, $\beta = \varphi e / (k\theta)$, with e = charge of an electron, k= Boltzmann's constant, and φ = thermionic work function, necessary to 'boil' out an electron. So a low value of θ, together with a high value of φ,

makes the emission easier. The emission is made simpler by a low value coupled with a high value. After being freed, the electrons hit the anode at a rapid rate of acceleration. Typically, this channel of electrons is seen in arc columns that are hotter than the surrounding area. One part of the arc column's heat is generated when thousands of electrons work together to increase the current carrying capability of each one. An additional source of heat is generated by high-velocity electrons and their kinetic energy. Heating occurs as a result of the anode being struck by these electrons. A protective ionized gas layer surrounds the electrons and electrostatic unit within the electron, combining with the negatively charged electrons and returning positively charged ions from the cathode to anode. There are three distinct zones of heat liberated in the arc column because of the properties of the electrons and the ions in it. This is seen in Figure 1.4.

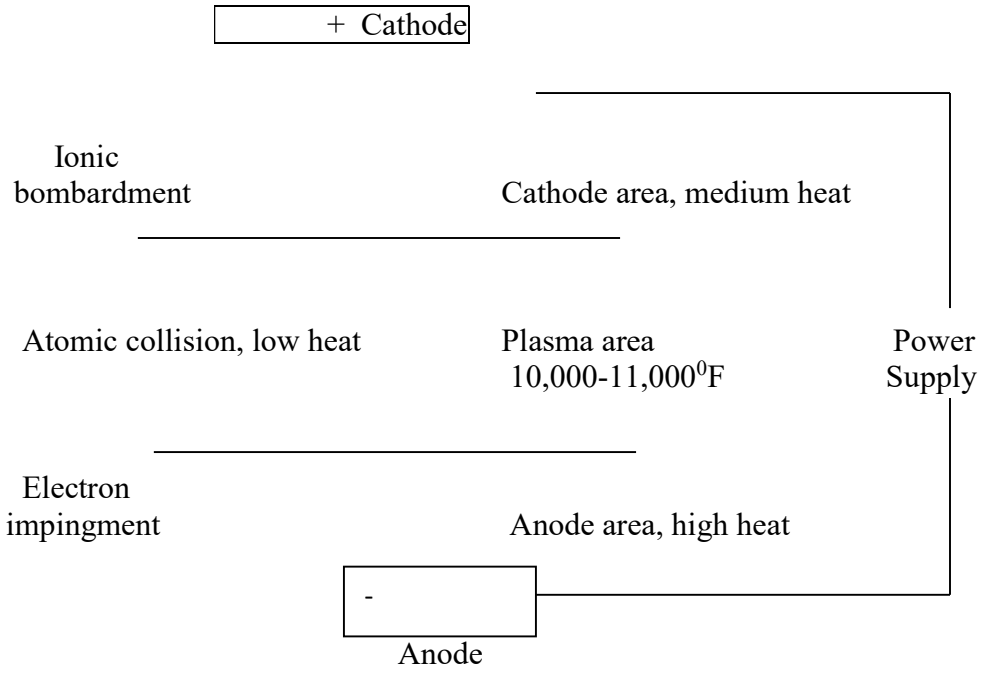

Figure 1.4 Heat liberation in arc welding [60]

Heat is released from the anode area due to the electron's impact with the anvil and the electron's ability to carry a significant amount of current. The collision of electrons and ions that pass through the column of ionized gas heats the plasma area. There is a lot of ionic bombardment in the cathode area, which causes the heat. The positive pole generates two-thirds of the heat, while the negative pole retains the other third. Arc melts the electrode and any material that comes into contact with the arc. When an arc is created, a small stream of molten metal rushes out of the

electrode tip and into a nearby puddle of molten metal. The arc melts and fuses the metal it encounters as it travels down the piece. Arc welding processes can be divided into several categories, with tungsten inert gas welding being the most widely used.

1.4 STAINLESS STEELS

In order to be considered stainless steel, an iron base alloy must include at least 10.5% chromium to meet this definition. Corrosion resistance is provided by the thin yet dense chromium oxide coating that forms on the surface of stainless steel. Alloy additions range from entirely austenitic to fully ferritic in the five varieties of stainless steels available. They can be welded using a variety of methods, including as arc welding, resistance and electron and laser beam welding, frictional and brazing. Stainless steels are generally considered to have good weldability. Cleanliness of the joint surfaces and any filler metal is required. Austenitic steels have a greater coefficient of thermal expansion than carbon steels; hence this must be taken into account to avoid distortion. Austenitic stainless steel has a low thermal and electrical conductivity, making welding easier. Welding heat requirements for stainless steel are lower than for carbon steel because the heat does not transfer away from a joint as quickly in stainless steel. Because resistivity is higher in resistance welding, a smaller current can be employed. When it comes to welding stainless steel, TIG welding is the preferred method.

1.4.1 TYPES AND COMPOSITION OF STAINLESS STEEL

The 200 and 300 series of austenitic stainless steels, the most common of which is type 304, are included. The two most common alloying metals are chrome and nickel. Steels made of ferritic stainless steels cannot be hardened. Types 405, 409,430,422, and 446 all fall within this classification. There are a number of martensitic stainless steels that have a similar composition to ferritic stainless steels, but they include more carbon and less chromium to allow heat treatment hardening. There are a number of different types in this family that can be found. Ferrite and austenite are present in almost equal proportions in the microstructure of duplex stainless steels. They have a chromium content of about 24% and a nickel content of about 5%. The 200, 300, and 400 numbering systems do not contain theirs. The hardening of precipitation A solution and ageing heat treatment can harden stainless steels since alloying additives like aluminium are

included in the steel itself. Additionally, they are subdivided into three groups based on the precipitation hardening stainless steels they include. The 600-series stainless steels are referred to as such (e.g., 630, 631, and 660).

1.4.2 WELDING OF STAINLESS STEELS

AUSTENITIC STAINLESS STEEL

Austenitic stainless steels contain between 16 and 26 percent Cr, 8 to 24 percent Ni + Mn, up to 0.40 percent C, and a few additional elements, such as Mo, Ti, Nb (Cb), and Ta. Typically, the ratio of Cr to Ni+Mn is tuned to provide a microstructure of 90-100 percent austenite. Good strength and excellent toughness across a wide temperature range and oxidation resistance to above 10000 F define these alloys (5380 C). Types 302, 304, 310, 316, 321 and 347 are all part of this collection. Table 1.1 lists the nominal composition of this and other austenitic stainless steels. In order to prevent heat cracking, the filler metals used in these alloys should have microstructures that include ferrite. This is accomplished by using type 308 filler for filler types 302 and 304 and type 347 filler for filler type 321. They should be welded with filler that matches. Type 308H filler can also be used to weld Type 347. Electrodes, solid bare wire, and wire cored with these filler materials have been coated. Type 321 is available in both solid and cored wire forms.

1.4.3 SELECTION OF THE TYPE OF STAINLESS STEEL

A particular type of stainless steel can only be used if it meets the specifications of the intended use. Generally, the most important factor to consider is the material's ability to withstand corrosion, tarnish, or oxidation at high temperatures. Mechanical qualities such as ductility and fatigue strength are also necessary for the stainless steel to meet these standards. A variety of stainless steel kinds and grades can provide the requisite corrosion resistance and mechanical qualities. Final choice should be made based on cost of lowest available alloy that meets service requirements. For the most part, stainless steels are chosen based on corrosion behaviour data collected by the equipment or component's designer, who typically has extensive training and

hands-on expertise with stainless steel alloys. The welding engineer's primary role is to select the filler material, the welding process, and the welding technique, not to select the base alloy.

Welding engineers need information on the part's service environment, expected lifespan, and acceptable corrosion level when selecting a base alloy. These are just a few of the many considerations that must be made when selecting a stainless steel for your application. Carbide precipitation in weld heat affected zones causes intergranular attack, which has been studied earlier. Creep strength, stress rupture, and oxidation resistance are all important considerations if the application will be operating at high temperatures. Welding engineers are responsible for designing the joints, selecting the weld filler metal, welding method, and welding technique after the stainless steel has been picked.

1.5 TUNGSTEN INERT GAS SHIELDED ARC (TIG) WELDING

1.5.1 TIG WELDING GENERAL PROCEDURE

GTAW, or Tungsten Inert Gas-Shielded Arc Welding, is a procedure that uses an inert gas to shield the tungsten electrode and the metal to be welded, creating an electric arc. An inert gas blanket pumped through the GTAW torch protects the heat-affected zone, the molten metal, and the tungsten electrode from ambient contamination. Argon is commonly used as an inert gas since it lacks any chemically active characteristics. For the purpose of protecting the weld, the shielding gas acts as a blanket. Inert gases like Argon and Helium do not react or interact with other gases. A welder can see the arc clearly because they have no odour and are transparent. Increasing the speed of a vehicle can sometimes be accomplished by introducing hydrogen gas. As high as 35,000° F (19,426° C) can be achieved using TIG welding. Only the workpiece is heated by the torch. It is possible to add filler metal manually in the same way as oxyacetylene welding does if it is needed to complete the weld. In addition to stainless steel, nickel alloys like MonelR and InconelR, titanium, aluminium and magnesium can be welded with GTAW. Dissimilar metals, such as copper to brass and stainless steel to mild steel can be welded together using GTAW. A typical TIG welding set up is shown in Figure 1.5.

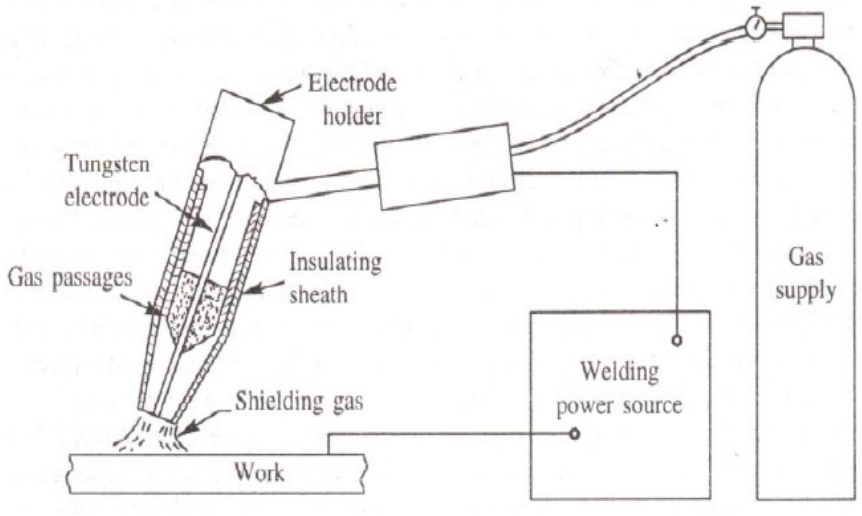

Figure 1.5 A typical TIG welding set up [60]

1.5.2 SELECTION OF TIG WELDING POWERSOURCE

Choosing a power supply for TIG welding is mostly influenced by the following factors:

1. What kind of metal is to be welded - (Aluminum, Steel, Stainless etc.)
2. Welding material thickness
3. a package solution that is appropriate for the welding application.
4. Components that enhance the overall functioning of the system.

Constant-current power sources are always employed. TIG welding can be done with either a DC or an AC power supply, depending on the application. The electrode can be either positive (DCEN) or negative (DCEN) when DC is utilised (DCEP).

1.5.3 TIG EQUIPMENT

A. ELECTRODES

A tungsten electrode is possible, but is more commonly made of thorium oxide (thoria ThO2) or zirconium oxide (zirconia ZrO2). Electrodes that have been coated with titanium dioxide are used

in DC applications. The electrodes that have been coated with titanium dioxide are utilized in DC applications. Although thoriated electrodes can be used for AC welding, zirconiated tungsten is preferable because it has a melting temperature of 33800 C and a boiling point of 59500 C, resulting in minimal vapourization in the arc and maintaining its hardness when red hot. With a ground grey surface to ensure the best collet contact, these non-consumable electrodes are available in diameters from 0.5 to 2.4 millimetres in zirconiated electrodes, as well as extra sizes for the 1 percent thorium-coated electrodes (e.g. 0.8, 8.0, 9.5 mm).

To start on DC, tungsten coated electrodes are preferable because of their higher current carrying capacity per diameter and the fact that they are easier to operate, even though pure tungsten electrodes can be utilized. A hemispherical end can be difficult to maintain when using the electrodes on an alternating current (AC). Hence, the reduced possibility of tungsten contamination makes zirconiated electrodes a popular choice for AC welding due to their strong arc starting characteristics. When welding aluminium and magnesium, zirconiated tungsten electrodes are the preferred choice. It's common practice to select an electrode size that falls somewhat in the middle of the spectrum for both electrode and work. An electrode that is too small can lead to tungsten contamination of the work, while an electrode that is too large can make arc control difficult. As a general rule, the electrode's lengths are 75 or 150 millimetres.

Sputtering and metal loss in the electrode tip can occur if the arc is created by first touching the base metal and then removing the electrode tip from the arc. Whilst tungsten oxide has a lower melting point than tungsten, this could result in the electrode becoming depleted more quickly. When the electrode is left to cool in the environment after welding, oxidation occurs. A shielding gas flow should be maintained after the arc has been extinguished in order to ensure that the electrode cools in an environment that protects it from being exposed to oxygen. The electrode tip needs to be cleaned and conditioned in order to ensure optimum weld penetration. Typical forms that can be employed are depicted in the figures below. Although it is feasible to use these electrodes without first preparing the tip, doing so improves the quality of the weld. A pencil-pointed tip is necessary when using an AC welding machine with an HF imbalanced machine to focus the HF current and make the arc easier to start. As soon as the arc is started, a tungsten ball forms on the tip, which lessens the effect of current rectification on the arc and helps to keep it stable in its current state.

The electrode would be conical with DCEN. In order to prevent contamination of the weld joint, it is critical that the tip concentricity be maintained while grinding. If this is not done, the gas flow will be uneven, resulting in puddle contamination. There are no conical points in pure tungsten electrodes, since the end of the electrode is prone to melt and contaminate the weld metal. You should instead form a full round ball at the point of your spear to avoid this. Figure 1.6 and Figure 1.7 show typical electrode tip shapes and preparing tungsten for DC electrode negative (DCEN) welding and AC welding using inverter machines.

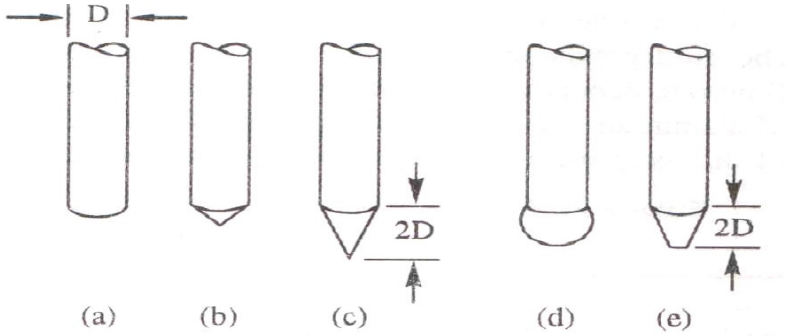

Figure1.6 Typical electrode tip shapes

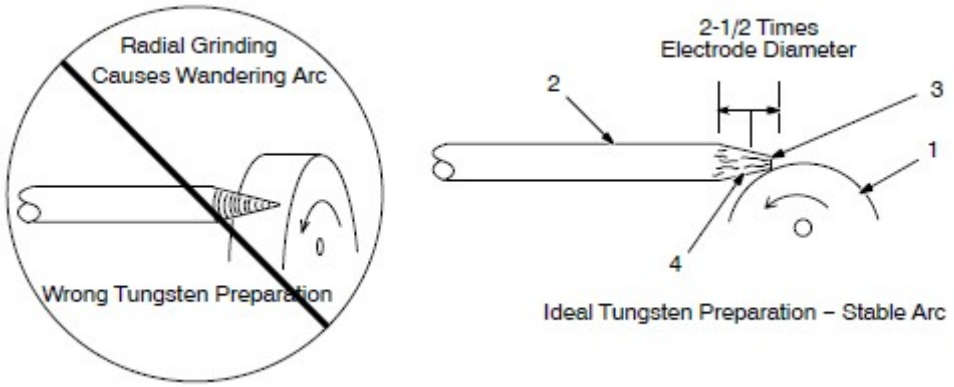

Figure 1.7 Preparing Tungsten for DC electrode negative (DCEN) welding or AC welding with inverter machines [59]

B. SHIELDING GAS

Metals such as carbon and alloy steels, stainless steels, aluminium and its alloys, magnesium and alloys, nickel and its alloys, zirconium, silver, etc., can be made with commercial pure argon (99.996%). Despite this, titanium requires a high degree of purity. When welding stainless steel and nickel alloys, argon with 5% hydrogen increases welding speed and penetration; nitrogen can

be used to weld copper. Due to its lower density, helium is more expensive than argon and a larger volume is needed to maintain proper shielding, and a slight difference in arc length causes significant variations in weld conditions. Helium can be used for aluminium and its alloys and copper. It is presently common practise to employ a combination of 30% helium and 70% argon, which provides high welding speeds. Aluminum helium automated DC welding provides deep penetration and high speeds. As current direction changes, so does the arc's physical properties, or arc polarity, as it is known.

C. TORCH

There are a wide range of torches on the market, from light-weight air-cooled to heavy-duty water-cooled models. Top loading compression type collet assemblies can be used with electrodes of different diameters. The collet can be loosened for electrode removal or repositioning without compromising the grip. The size of the torch and electrode diameter must grow as the thickness of the plate to be welded increases. Welding in tight spaces calls for compact, light air-cooled torches with current ratings of 75 A DC or 55 A AC. These torches can have a pencil or swivel head. In general, these have a 0.8, 1.2, and 1.6 mm-diameter cotter pin. 1.6 mm collets are used on larger, air-cooled torches with a continuous or intermittent 75A DC or AC rating, as well as a continuous 100A intermittent rating. Water cooled shields can be used on torches rated at 300 A intermittent with electrodes ranging in diameter from 1.6 to 6.35 mm. Heavy duty water cooled torches use electrodes with a diameter greater than 6.35 mm and have a water cooled nozzle rated at 500 A AC or DC continuous. Adding a gas lens can improve the torch's gas coverage and make it easier to use or see. When the flow of gas from the nozzle is turbulent, the electrode can be adjusted to protrude up to 4-9mm beyond the nozzle. Typical air cooled torch is shown in Figure 1.8.

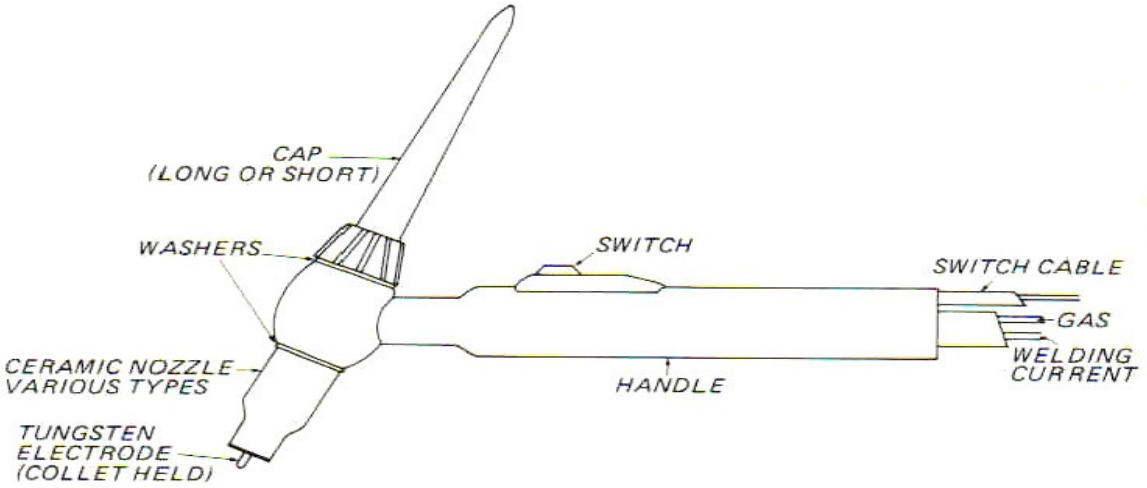

Figure 1.8 Typical Air cooled torch [59]

D. GAS REGULATOR, FLOWMETER AND ECONOMIZER

The argon cylinder's pressure is reduced from 175 to 200 bar to 0-3.5 bar by the gas regulator before being supplied to the torch. When using a needle valve-operated flowmeter to manage the argon flow rate, the flow rate can range from 0-2100 litres per hour. For example, a welder can place the economizer next to his or her torch to cut off gas and water supplies when the torch is suspended from a lever on the device. The HF unit can alternatively be controlled by a micro-switch that is activated by the lever.

E. ADDITIONAL EQUIPMENT

A variety of add-on devices are compatible with transformers and rectifiers already in place. With a pulse generator on board, the unit can be used with either an AC or DC arc welding source or a thyristor controlled rectifier power unit. If connected to a DC power source, the pulse generator is only utilized to start the arc, and it is immediately shut off after the arc has been established. When connected to an AC power supply, the pulse generator ensures that the arc is ignited without the need for contact and that the arc is re-ignited during the welding procedure. Additional features include: remote control, one-knob current control, soft start, crater-fill, and other features that may be controlled remotely.

1.6 INSPECTION AND TESTING OF WELDS

To meet demand, good quality weld is preferred, and to maintain good quality weld, inspection at every step is required to check for defects or improper processes. There are three stages to check for proper welding. Prior to welding, removing unwanted things that may affect weld quality, maintaining input parameters (gas flow rate, welding current, arc gap, welding speed, welding voltage, etc.) that affect heat input in the welding process and protecting the weld pool from atmospheric contamination, and removing slag, peening, and post welding treatment. Keeping these three steps in mind will result in a quality weld. Several inspections in the form of different tests are performed on the prepared weld to check how well it has been prepared. There are two types of welding joint testing methods: destructive and non-destructive.

1.6.1 NON-DESTRUCTIVE TEST

Visual, ultrasonic, and radiographic non-destructive tests for welds (X-ray). All non-destructive tests can detect weld-meant flaws.

This type of testing can only detect surface-breaking discontinuities, or discontinuities that are open to the penetrant's surface. It can't detect internal porosity or fusion defects that are sealed within the weld body. It's not suitable for testing rough or porous materials because false results can hinder interpretation. Compared to unassisted visual inspection, this type of inspection is more likely to detect hairline cracks and micro surface porosity. This inspection method can be used on ferrous and nonferrous materials.

During fluorescent penetrant inspection, a highly fluorescent liquid is applied to the inspection area. The developer draws the penetrant to the surface, and the black light inspects the weld. Inspectors can detect penetrant traces on surfaces by contrasting the fluorescent material with the object.

In this physical weld testing radiographic method, defects like cracks, blowholes, and improper fusion zones are revealed. Radiography relies on the ability of X-rays and gamma rays to pass through metal and other opaque materials and record the radiant energy transmitted. We keep an

x-ray tube on one side and a sensitive emulsion x-ray film on the other. Defects in the metal plate appear as dark spots and bands. An operator familiar with these inspection methods can interpret these flaws. X-ray radiographic procedures is shown in Figure 1.9.

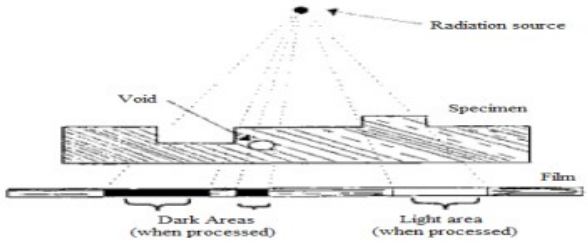

Figure 1.9 Radiography inspection [59]

1.6.2 DESTRUCTIVE TEST

Destructive weld testing involves physically destroying the weld to evaluate its properties. This testing method is widely used in many applications.

Tensile Strength Test: This test measures the tensile strength of a welded joint. In the testing machine's jaws, a segment of the welded plate is to be tested. The test sample's width and thickness are measured beforehand. Before testing and calculating, multiply the width and thickness. The tensile physical weld strength test specimen is now mounted on a machine that will pull hard enough to break it. The testing machine can be portable or stationary. The figure depicts a portable hydraulic testing machine strong enough to pull and bend the specimen. The load in pounds is visible on the gauge while testing this machine. The stationary machine shows the balancing beam load. The load is always recorded at the break. The tensile strength is calculated by dividing the specimen's break load by its initial cross-sectional area. The specimen must pull at least 90% of the base metal tensile strength. Tensile stress of test samples determines shearing strength of longitudinal and transverse fillet welds. The test sample ruptures and the maximum load is marked. This test can determine the weld joint's yield strength, ultimate tensile strength, ductility, percentage elongation, Young's modulus, etc.

Bend Test Method: A predetermined bend radius is applied to a specimen. A welded joint's ductility and strength can be evaluated using bend tests. Plunger test machines or wrap-around bend test jigs are commonly used to perform these tests transverse to the weld axis. Weld face and root tension is used to perform face and root bend tests. When testing thick plates, the weld cross section bends in tension. Welding methods and welder performance testing most often use this term. Liner fusion faults, which are common on the plate surface during testing, can be detected with this form of testing. In these guided bend tests, the quality of the weld metal at the joint's root and face is determined.They assess the weld's fusion, penetration into the base metal, and efficiency. This type of testing is jig-able. The test specimens are machined from the welded plates. Our bending jig should be able to bend these specimens. The test specimen is placed on the die support, which is the jig's lower part. The hydraulic jack's plunger pushed the specimen in, revealing the die shape.

Hardness is defined as the resistance to localised shift indentation. We can say wear, abrasion, and indentation resistance. However, this non-destructive test is rarely used in the field. The hardness test is used to control the properties of materials as the desired hardness is achieved. The test determines the weld metal's hardness. Examine the weld joint carefully to determine the effect of welding heat on the base metal's baseline properties.

1.7 WELDING DEFECTS

Welding defects are irregularities formed in the weld metal due to incorrect welding processes or welding patterns.

Weld Crack: The most dreaded of all welding flaws. These can occur on the surface, inside the weld material, or in heat affected zones. Hot Crack occurs during crystallisation of weld joints, where temperatures can exceed 10,000°C. Cold Cracks occur at the end of welding when the temperature is very low. A cold crack can appear hours or days after welding. Undercut: When the metal base melts away from the weld zone, a groove in the shape of a notch forms. It reduces joint fatigue strength. Metal drops expelled from a weld and stuck to the surface are known as Spatter. Porosity occurs when gas or small bubbles get trapped in the welded zone. This defect occurs when the weld face extends beyond the weld toe. The weld metal rolls and forms a less

than 90 degree angle. The crater does not fill before the arc breaks, causing the outer edges to cool faster than the crater. This causes a stress and a crack. Slag inclusion: Slag in the weld reduces the material's toughness and metal weldability. This reduces the weld's structural performance. Slag forms on the weld surface or between the welding turns. Incomplete fusion occurs when the welder miss-welds the material and the metal pre-solidifies, leaving a gap that is not filled with molten metal. Metal drops ejected from the weld stick to the surrounding surfaces, causing splatter. Spatter can be reduced by correcting the welding condition and removed by grinding. In the present study, visual inspection, radiography tests and tensile tests have been performed. The quality of weld has also been evaluated through study of the microstructure of the weldment. The photographic view of some of the welding defects is shown in Figure 1.10

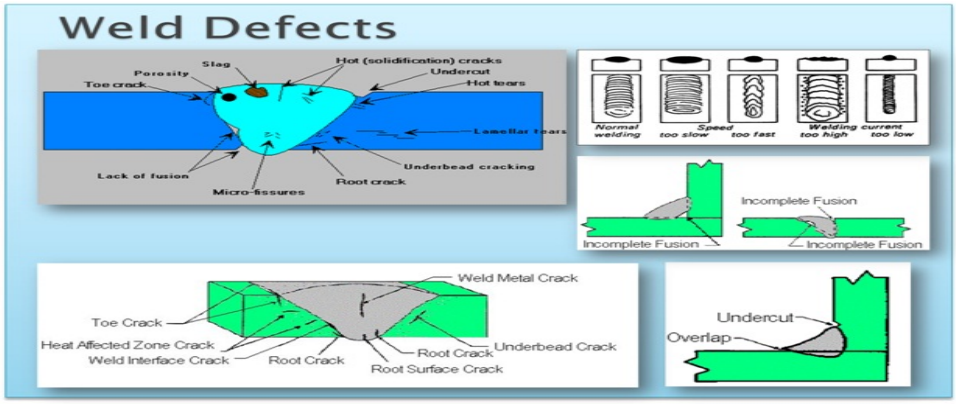

Figure 1.10 welding defects [59]

1.8 LITERATURE REVIEW

The weld quality examiners have constantly been on the lookout for ways to improve the weld. Numerous components of this ongoing search are at play. Examples include the examination of welding in some specific material, for example. This means that for a given material, weld defects can occur due to numerous causes that will have an impact on the weld quality.

According to Wang et al. [1] welding parameters influence the morphology, microstructure, tensile property, and fracture. The welded junction's tensile, yield, and elongation properties all improve as the welding current increases. Welding speed and current both enhance the heat input.

It has the ability to enhance the amount of free dendritic crystals, decrease the amount of columnar crystals, and expand and deepen the welding pool. Strength and elongation may be harmed by an increase in impulse frequency. Tensile fracture has dimples in it that make it ductile. By integrating microstructure and tensile properties, the best process parameters can be achieved. The welding current is 8090A and the welding speed is 25 cm/min..

As reported by Izzatul Aini et al. [2], robotic gas metal arc welding measurements of penetration, microstructure, and hardness in 6mm-thick mild steel were examined. By increasing the welding current, we were able to achieve penetration depths of 90, 150, and 210 A, respectively. Welding current, together with welding speed and arc voltage, affects penetration. The toughness of the weld bead increases at lower currents and decreases as the current rises.. The microstructure's grain boundaries narrow as welding parameter variables change.

An investigation of the mechanical characteristics of AA6351 weldments produced by non-pulsed and pulsed current welding at 3Hz and 7Hz is presented in this paper by Indira Rani M and R N Marpu [3]. They found that pulsed current welding gives superior welds and tensile strength over non-pulsed current welding because pulse current allows greater penetration and fusing of filler material with the parent material. Weldments were found to be flawless as well.

Erdal Karadeniz [4] found that different welding settings had varying effects on the penetration of Erdemir 6842 steel that was welded by robotic gas metal arc welding at 2.5 mm thick. Increased welding current between 95 and 115 A results in a 0.0225-mm increase in penetration depth for every 1 A increase in current. In addition, arc voltage boosts penetration by 0.02-0.12 mm for 22-26 V, however the effect is less significant than that of welding current. The penetration value rises from 0.03 to 0.08 mm between 40 and 60 cm/min and then gradually decreases after that. Macro-photographs were used to accurately measure bead heights and penetration depths in a variety of configurations. Using 105 amps, 24 volts, and a welding speed of 80 centimetres per minute appears to be the best combination for penetration and weld joint. Welding current has a stronger impact on penetration than arc voltage and welding speed.

Weldable mild steel specimens measuring 50mm by 40mm by 6mm were tested by P. Tewari et al. [5] under various metal arc welding settings. The deepest penetration, 5.41 mm, was achieved at 110.39 mm/min and a heat input rate of 1369.68 J/min when welding speed was used as a customizable parameter. In order to maximise penetration, increasing travel speed and

maintaining the arc voltage and current constant will help until the optimal speed is reached. An increase in the speed beyond this point will reduce the penetration.

Several factors, including the kind of power supply, current, gas flow rate, electrodes, filer wire, TIG machine characteristics, and shielding gases were examined by N. Jeya prakash and M. Arun prasath [6]. Arc stability, arc penetration, and defect-free welds are all dependent on these variables. The cleanliness of the equipment, supply, base metal, tungsten end and tip shape, etc., are all critical considerations for achieving high-quality welding. There are torches ranging in power from 10A to 450A available. Depending on the parent material, the filler rod should be chosen. The automation or mechanisation of the TIG process has numerous advantages, as explained by the study's authors.

Using Shielded Metal Gas Welding methods, Kishore et al. [7] attempted a qualitative examination of the impact of process parameters on the welding of AISI1040 steel (MIG and TIG). Arc voltage, arc current, welding speed and distance from the nozzle to the weld are the most important control parameters for weld quality. There is a direct correlation between plate thickness and the thickness of the backing plate. For 3mm and 5mm plates, MIG welding required currents of 150A and 180A, respectively, to avoid LOP. For TIG welding, the current levels are 65 A and 80 A in this case. Only 0.45 metres per minute is acceptable for 3mm plate, while the nozzle tip distance should be kept at around 10 millimetres. A nozzle tip distance of 12mm for a 5mm plate maintains the 0.35m/min velocity in MIG welding.

R. Patil and C. A. Waghmare Waghmare [8] examined the influence of several welding parameters, including welding current, welding voltage, and welding speed, on the UTS of AISI 1030 mild steel material during welding by R. Patil and C. A. Waghmare [8]. When it comes to determining the material's weldability and optimising the welding settings, we use the Taguchi method and orthogonal array, signal-to-noise ratio, and analysis of variance (ANOVA). Speed of welding, among other parameters, has a considerable impact on tensile strength. The ultimate tensile strength of the welding joint can be increased by raising the welding speed and reducing the current.

With regard to GMAW (gas metal arc welding) technology, the influence of different welding settings on the welding joint quality and the shape of welding bead was evaluated by Mehdi Heidari [9]. The experimental matrix is constructed using Taguchi's method, which is then fitted

with data collection and regression processes to develop mathematical models. Following an analysis of variance (ANOVA) procedure, the best-fitting model is identified. ANOVA shows that the data are best fitted by a curvilinear model in this case. A Simulated Annealing (SA) optimization technique is then used to the selected model. Using a Simulated Annealing technique, a weld bead's error function was reduced by a factor of two.

Welding parameters have an impact on the quality and strength of welded joints, according to Satyaduttsinh P. Chavda et al. [10]. The Taguchi method was used to collect the data. There are two methods used to better understand the welding characteristics of medium carbon steel: an orthogonal array and analysis of variance (ANOVA). Welding current, arc voltage, welding speed, type of shielding gas, gas flow rate, wire feed rate, and electrode diameter all have an impact on the mechanical characteristics and weld bead shape of the weld. When the welding settings are changed, the grain boundaries of the microstructure are altered, resulting in a greater penetration depth.

The cooling curves (TTP) of 6063-T5 aluminium alloy plates welded with MIG were numerically studied by Jose L. Meseguer-Valdenebro et al. [11]. The Taguchi design makes use of orthogonal arrays to plot the course of the experiment as it relates to modifying the various aspects of welding. We use a L4 array because the experimental design contains two variables (power and welding speed) and two levels for each. ANOVA is used to assess the importance of the analysed welding parameters.

Welding current, voltage, and shielding gas flow rate were all evaluated by Diganta Kalita and Parimal Bakul Barua [12] to see how these three parameters affected the tensile strength of Grade C20 Carbon Steel and ER70S-4 electrode weld joints. Taguchi's Orthogonal Array L9, with three layers of data for each factor, is used in the experiment. In this study, the results show that welding voltage has a large impact on weld tensile strength mean and variation, contributing 87.019% and 85.398%, while welding current only has an impact on the mean (10.807 percent contribution).

Chandresh N. Patel and Sandip Chaudhary [13] welded ASI1020 or C20 with MIG and TIG. Experimentation and data gathering use the Full Factorial Design method, and experimental data is optimised using grey relational analysis (GRA). MIG welding inputs include welding current, wire diameter, and wire feed rate; the output is hardness. ANOVA and GRA are used to

determine each input parameter's contribution to obtaining optimal circumstances. MIG welding contributes 94.01 percent of welding current, 0.402% of wire diameter, and 0.016 percent of wire feed rate. TIG welding contributes 73.36 percent to welding current, wire diameter is 23.90 percent, and inaccuracy is 2.74 percent. Human inefficiency and mechanical shaking cause this inaccuracy.

An investigation into the effect of weld settings on penetration was conducted by Ambekarand D. Sunil R. Wardhokar [14]. For the Martensitic stainless steel AISI 410 work piece, an orthogonal array Taguchi method study was undertaken to optimise the gas metal arc welding (GMAW) process parameters. Analytical methods such as ANOVA and the S/N ratio are used to identify the most important factor in determining the best parameter setting among the effects of welding parameters, such as welding speed, welding current, and wire diameter. Wire diameter = 1.2 mm, welding speed = 60 cm/s, and welding current = 110 amps have been proven to be the best settings for this machine. According to the calculations made using a standard error of 4.90%, welding speed contributes 46.61 percent, welding current contributes 21.24%, and wire diameter contributes 27.25% to the final MIG welding percentage. Both human inefficiency and machine vibration are to blame for this inaccuracy.

Tungsten inert gas (TIG) and metal insert gas (MIG) welding of various materials was thoroughly examined by Neha Agrawal et al. [15]. Various weld metrics, such as tensile strength and hardness, as well as other important structural features, are evaluated in this study. Welding at higher speeds with a higher current enhances the mechanical properties of the weld metal. TIG welding's tensile strength, fracture porosity, and ductility are all improved when using an alternate shielding gas. Weld failure progresses from the weld toe to the weld root under uniaxial fatigue pressure. The size of the heat-affected zone is reduced when stainless steel GTAW welding is performed with a low heat input. Pressure changes from tensile to compressive as it moves closer to the core.

In Gas Tungsten Arc Welding (GTAW) of dissimilar metals, Kumar Rahul Anand and Vijay Mittal [16] studied equipment and welding factors such as welding current, gas flow rate, welding speed, electrode, etc. as inputs that affect outputs such as tensile strength and weld hardness.

When it comes to the mechanical qualities of SS304H, welding factors such as YS, UTS, Toughness, and Vicker hardness were studied by Saadat Ali Rizvi [17]. (VHN). Using the

Taguchi method, a L9 orthogonal array is used to conduct an experiment and optimise welding settings. Different welding parameters, such as wire feed speed, welding current, and gas flow rate, have an effect on weld quality, which may be measured using SNR and ANOVA. Mechanical characteristics such as tensile strength, toughness, Vicker hardness (VHN), and fracture mode were evaluated to evaluate the weld quality of SS304H. In terms of the weldment's strength, welding voltage has a significant impact, whereas the gas flow rate has little impact. 23 V, 350 IPM wire travel speed, and 20 l/min gas flow rate were found to be the best process parameters.

Gas Tungsten Arc welding parameters for Inconel 825 are being optimised by Prabaharan et al. [18]. As part of a welder's set of parameters, the welding voltage, current, gas flow rate, and the distance from the nozzle to the plate must all be taken into consideration (). Increases in welding current, gas flow rate, and torch angle increase weld deposit area whereas increases in voltage and nozzle-to-plate distance decrease it, according to an ANOVA analysis of the experimental data.

Factorial testing is used by Omar Bataineh et al. [19] to identify and improve the most important factors that affect weld joint strength. Researchers looked examined arc voltage as well as filler feed and gas flow rates in addition to specimen edge angle and preheat temperature. Arc voltage and filler feed rate are the only two variables that stand out in the experimental data after an analysis of variance (ANOVA). Arc voltage and filler feed rate were determined to be 24 V and 7 in/s, respectively, based on regression analysis for highest mean weld strength.

For MIG welding procedures requiring specific applications, a case study by Mohan B. Raut and S. N. Shelke [20] sought to determine the most effective design. When using MIG welding, the most important characteristics to consider are the amount of current being applied to the metal, the voltage at which the current is applied, the speed at which the metal is being welded, and the amount of filler wire being fed into the machine. Taguchi, Orthogonal Array, Signal-to-Noise Ratio (S/N ratio), and analysis of variance can be used to determine welding characteristics and optimization variables (ANOVA). Taguchi optimization's effectiveness was proven by conducting additional experiments. By a factor of 2.13, the S/N ratio improved. The ideal welding conditions are a penetration of 5.25 mm and a S/N ratio of 14.40. The experimental value for the S/N ratio is 14.40.

Using a 0.8 mm diameter copper-coated mild steel wire, Shekhar Srivastava and R.K. Garg [21] studied the effect of various process parameters on the welding of IS: 2062 mild steel plate. It is the mechanical properties of the weld metal and the heat-affected zone (HAZ) that determine the quality of the weld. This is directly tied to the type of welding and its process parameters. There are many variables that affect the weld's mechanical properties such as tensile strength or hardness that have to do with the weld's bead geometry. These include the heat affected zone (HAZ), bead width, bead height (BH), penetration and area of penetration (PA), arc travel speed (ART), contact tip–work distance (CTWD), shielding gas type (SG), etc. Analysis of variance (ANOVA) is used to assess the importance of process variables. Welding process efficiency can be improved using Response Surface Methodology as well.

Stephen A. Akinlabi et al. [22] examined TIG/MIG welding to improve the microstructural, mechanical, and metallurgical attributes of designed materials. A hybrid welding process improves the mechanical and metallurgical qualities of welded structures. The hybrid TIG/MIG technology hasn't been properly researched despite its promise. Its applications and methods are limited since its process parameters are not well known. Most research explore geometric factors like tensile and hardness. Numerical modelling can be used to examine and assess TIG/MIG hybrid welds.

For the parametric multi-objective optimization of TIG-MIG hybrid welding of AISI 1008 mild steel joints, Cynthia Samuel Abima et al. [23] investigated. Taguchi's L-9 orthogonal array is used in the experimental design matrix. The Grey relational grading system uses first- and second-order regression for mathematical models and process parameter optimization. ANOVA analysis shows that gas flow rate had the greatest impact on the results, accounting for 39.77 percent of the variation. The coefficient of determination (R2) of the second-order regression models for the two answers was higher than that of the first-order models, indicating that they were the best fit for the process. Voltage (MIG) = 25 V, Current (TIG) = 180 A, and gas flow rate = 19 L/mm were found to be the best parameters for multi-objective optimization using the grey-based Taguchi technique.

Research by Vasantharaja et al. [24] found that TIG and A-TIG welding procedures had varying effects on the microstructure, residual stresses, and deformation of stainless steel weld joints of 16 mm thick (double V grove and y grove). The radiographic examination of all welded joints found

no defects. Microstructural characterization was carried out with the aid of an optical microscope. An ultrasonic method using LCR waves was used to quantify residual stresses, and a height gauge was used to measure the distortion. The microstructures, peak residual tensile stresses, and distortion patterns of the three weld joints are all different from one to the other. The ferrite concentration was lower, the peak tensile residual stress was lower, and the grain size was coarser in double-sided A-TIG weld joints. The ferrite concentration was larger, the grain size was smaller, and the peak tensile residual stress was higher in double-sided TIG weld joints. Relatively low angular distortion values were found in double-sided A-TIG and TIG weld joints, while Y-grooved joints had the highest values.

Welding TIG joints of two identical stainless steel grades was studied by V.Anand Rao and Dr.R.Deivanathan [25]. Microstructure of 310 austenitic stainless steel welds is studied using various grades of stainless steel filler material, and many variables such as welding current, filler materials, welding speed, and so on, are analysed and optimised. It was found that a welding current of 120A and a 309L electrode resulted in the highest tensile strength of 454.6MPa, while an 80A current and a 316L electrode resulted in the lowest. Welding 120A current through a 316L electrode produced a minimum bending strength of 646.55 MPa, while welding 120A current through a 347 electrode produced just 211.37 MPa. The tensile and bending strength of 309L filler material has been improved.

Optical and electron scanning microscopes were used by M.Anuradha et al. [26] to examine the weld's microstructure and fracture surface. Using experiments and a response surface approach model, they investigated how welding parameters affect mechanical qualities when Inconel 781 is TIG welded to ANSI 4140 steel. Welding strength was shown to be optimally enhanced when high welding speed was combined with low welding current. The maximum hardness was found in the heat affected zone of AISI 4140, where a martensitic microstructure developed after welding.

Autogenous TIG welding of an Al-Cu-Mg-Mn alloy was investigated by A.F. Norman et al. [27]. Due to the abundance of homogeneous nucleation sites, the researchers found that a combination of high welding speeds and low power densities was necessary to promote the nucleation and growth of equiaxed grains in the weld pool. Dendritic fragments and TiB2 particles that survived in the weld pool are combined to create nucleants. Because of the quicker cooling rates at the

centre of the weld compared to the fusion boundary, we can see the finest microstructure. The dendritic secondary arm spacing shrank as welding speed increased because the rate of cooling at the weld's core increased. Dendritic side arm spacing and micro-segregation behaviour have been studied using quantitative EXD analysis. A Scheil-type behaviour is evident in this micro-segregation of dendritic side arms, which is in line with the absence of significant solid-state back diffusion.

Weld quality was evaluated by Narayana et al. [28] using various TIG welding conditions. By analysing the tensile strength of TIG-welded AISI 4140 stainless steel, Taguchi developed the L9 orthogonal array optimization technique. With the help of the regression model, the researchers were able to establish a link between Tungsten Inert Gas welding of AISI 4140 stainless steel plates and penetration. There is a stronger correlation between weld current and filler diameter and weld speed, as shown by the ANOVA analysis of the data.

Welding with activated flux TIG (ATIG) instead of standard TIG has been studied by Paulo J. Modenesi et al. [29]. It was found that using a small layer of an active flux during ATIG welding greatly increases the penetration of the welds made with the AISI 304 austenitic stainless steel specimen. With a thickness of 5 mm, it was possible to get a full penetration weld in austenitic stainless steel plates without any preparation. 230A of current was supplied, the arc voltage changed by 3%, and the voltage fluctuated by 1 V. The ATIG welding technology performed similarly to regular TIG welding in terms of operational features. Due to the high electronegativity components that confine the arc in a way similar to plasma arc welding, this good penetration effect is caused by the capture of electrons in the outer sections of the arc. Fluxes with only one component can be used for ATIG welding, which has a far higher penetration rate than TIG welding.

The advantages of activating flux in TIG welding over other arc welding processes were examined by Akash B. Patel and Professor Satyam P. Patel [30]. With a L9 orthogonal array, Taguchi techniques were used to determine the ideal settings for each TIG welding parameter. The influence of activating flux on the mechanical properties of TIG-welded 321 austenitic stainless steel was studied using SiO2 and TiO2 oxide particles. According to the results of the experiments, welding current and flux % are the most effective and improve penetration among the three basic parameters of welding current, gas flow rate, and flux proportion. As a result, by

reducing the grain size, the flux improved the heat-affected zone's penetration and mechanical properties.

Ahmed Khalid Hussain et al. [31] examined the effect of welding speed on the tensile strength of a TIG-welded aluminium AA6351 V-butt joint. As the V butt joint's bevel height increases, the weld bead's depth of penetration decreases. At 6.0 cm/sec weld speed (400 bevel and 1.5 bevel height), maximum tensile strength was 230 Mpa, suggesting that the weldment is weaker than the base metal. A lower range of weld speed is preferable for maximal tensile strength, according to the association between the two. Bevel angles between 300 and 450 degrees are recommended for strength. In the heat-affected zone, force increased as heat input decreased.

Pasupathy and V. Ravisankar [32] studied the effects of welding current and speed on dissimilar welding of low carbon steel and AA1050. Data is collected using the Taguchi method and analysed using orthogonal array, signal-to-noise ratio, and analysis of variance to optimise welding settings. The measured experimental strength is 61.37MPa and the S/N ratio is 16.45.

Welding current, speed, voltage, and pulse on time were all examined by Asif Ahmad and Shahnawaj Alam [33]. Two- or three-dimensional representations of interplay between mean response and input control parameters can be analysed and depicted using Response Surface Methodology (RSM). Mathematical models developed by RSM using design expert 11 and complete factorial central composite design answer the problem (CCD). Using the appropriate combination of input parameters, penetration depth is examined. Welding speed was shown to have the highest F-value in this ANOVA investigation, indicating that it is the most important process parameter for performance. Process parameters include 160A of welding current, 20V of welding voltage, 193 mm/min of welding speed, and a pulse on time of 40%. The predicted DOP was 5.53 mm, and the experimental DOP was 5.40 mm, proving the validity of the regression model that was built.

Multi-objective optimization using grey relation analysis was the focus of Arun Kumar Srirangan and Sathiya Paulraj [34]'s research on the Incoloy 800T welded tungsten inert arc welding process using N82 filler wire of 1.2 mm diameter. The welding current, voltage, and welding speed were used as input parameters in L9 orthogonal array experiments. The ultimate tensile strength, yield strength (at room temperature, 7500 C), and impact toughness were all chosen as the quality goals. While taking into account a wide range of output variables, grey relation analysis was

utilised to optimise input parameters simultaneously, and the best parameter combination was A2B1C2, i.e. 110 A of current, 10 V of voltage, and 1.5 mm/s of weld speed, Welding speed (30%), voltage (20%), and current (58%) were found to have the biggest influence on multiple responses based on the ANOVA results (12 percent).

For an optimum parametric combination that results in favourable bead geometry for welded connections, Ugur Esme et al. [35] used the Grey relation analysis and Taguchi technique. Using Taguchi's orthogonal array, sixteen experiments are undertaken to find the objective function to be optimised. TIG welding bead shape, bead width, bead height, penetration, area of penetration, as well as the breadth of the heat-affected zone and the tensile stress are taken into consideration when selecting the objective function. Grey connection analysis is used to address a multi-response optimization problem. In this study, it was found that Grey relation analysis and the Taguchi approach were able to greatly improve the specified parameters.

Jay J. Vora et al. [36] studied the possibilities of multi-response optimization applying integrated response technique with the JAYA algorithm to optimise the A-TIG welding process parameters when using TiO2 flux on carbon steel. Welding current, air gap, and travel speed are examined as input parameters; penetration depth, depth-to-width ratio, heat input, and total heat affected zone width are evaluated as output performance characteristics. Research is to determine exactly what input parameters are needed to achieve the desired performance characteristics at the same time. Other strategies, such as teaching-learning-based optimization, TLBO, and so on, are compared to the outcomes of the JAYA algorithm. Results show that A-TIG welding increases penetration in carbon steel, with a high penetration of more than 8 mm achieved with flux TiO2 under other welding conditions. An empirical model for the response parameter was found to provide a robust and reliable optimization framework for both single- and multi-objective problems.

During TIG welding of 304 stainless steel and mild steel, researchers Vishal Chaudharie et al. [37] studied the effects of current, voltage, and gas flow rate on the tensile strength and hardness of the joint. This dissimilar joint is studied using Taguchi's method of optimization, Taguchi orthogonal array, signal to noise (S/N) ratio, and analysis of variance (ANOVA). The welding parameters are optimised using these methods. 150 amps of current, 24 volts, and a gas flow rate of around 10 cubic feet per minute are the best weld strength criteria. These are the ideal

specifications for hardness, with a current of 150 amps, 22 volts, and 12 litres per minute gas flow.

G. Sathish Kumar et al. [38] employed Taguchi's orthogonal array L9 to examine the influence of welding current, travel speed, and gas flow rate on TIG welded samples of Aluminum 6082 as base material and AA5356 as filler wire with a 2.4 mm diameter. Increased welding current increases tensile strength, decreases hardness, and improves metal penetration. Travel speed and gas flow rate improve tensile strength more than hardness.

Sriramoju Avinash et al. [39] used Taguchi's approach to study welding quality. L9 array optimises mechanical qualities of SS 304 and Monel 400 dissimilar joints welded using ERNiCrMo-3 filler rod. Grey relation analysis optimises multi-response simulation factors. ANOVA is also used to determine the effect of input parameters on the sample characteristics. Optimal base current, peak current, and pulse frequency are 90 A, 180 A, and 4 Hz. Frequency affects output response, base current, and peak current, according to ANOVA.

Balram Yelamasetti et al. [40] examined dissimilar welded joints of AA6082 and AA7075 with ER4043 filler wire using Taguchi's technique. Welding current, filler wire diameter, and root gap were inputs; mechanical characteristics and bead geometry size were outputs. L9 array was employed to optimise the output response, and grey relation was used to optimise multi-objective input parameters. ANOVA determines welding parameter significance. The 8th trail delivers the best output for 210 A current, 2.4 mm filler wire diameter, and 2.0 mm root gap. Welding current affects production by 36.75 percent, filler diameter by 35%, and root gap by 22%. Additional tests confirmed the results.

K. Mahendra Babu et al. [41] conducted an experiment to examine the effect of various process parameters on weld bead geometry, weldment quality, and mechanical-metallurgical features. Taguchi's L9 orthogonal array was utilised to construct the experimental plan to TIG weld two aluminium alloy 6082 sheets with a 1.5 mm gap. Grey relation analysis optimises experimental outcomes. Maximum tensile strength is 145.85 MPA at 35mm/min, 190 Amp, and 2 mm filler rod. With grey regression and s/n ratio, travelling speed has a larger effect on tensile strength than filler rod diameter.

V. Vinoth et al. [42] optimised TIG welding settings for 316 stainless steel. Taguchi's approach is used to develop experimental plans, with current, welding speed, and gas flow rate as inputs and

tensile strength, impact strength, and corrosion rate as responses. Grey relation analysis optimises input parameters to achieve target mechanical properties at 150 A, 190 mm/min, and 15 L/min gas flow. Current, welding speed, and gas flow rate had a considerable effect on output responses, contributing 42%, 39%, and 18.8% correspondingly. Error contributed 0.2%.

M. Vasudevan et al. [43] conducted an experiment to assess and optimise A-TIG welding settings for 9Cr1Mo steel weld joints. Genetic algorithm (GA) model is utilised to identify optimum process parameters, and ANN is used to find correlation between output response such as penetration depth, weld bead width, and HAZ with input parameters such as current, voltage, and torch speed. GA code uses ANN model objectives.

Joby Joseph et al. [44] optimised activated TIG welding of sintered hot-forged AISI 4135 steel produced by powder metallurgy. Taguchi's L9 orthogonal array is utilised to develop the experimental plan and create the regression equation. The process parameters are then optimised using genetic algorithm (GA) and simulated annealing (SA). Current, voltage, welding speed, and gas flow rate are process factors, and the output reaction is tensile strength. GA and SA can correctly calculate the optimal welding parameter for desired tensile strength. Low voltage (11.5V), low current(60 A), medium welding speed (60 mm/s), and gas flow rate are the optimal parameters for A-TIG welding in this investigation (10 lpm).

L. Srinivasan et al. [45] optimised 115DCV6 TIG welding settings. It's an aerospace-grade high-strength, low-alloy steel. Current, voltage, welding speed, shielding gas flow rate, and output responsiveness when performance criteria were modified. Four learning techniques, Batch Back Propagation (BBP), Quick Propagation (QP), Incremental Back Propagation (IBP), Legvenberg-Marquardt (LM) back propagation utilised to train the model, and LM is found to be more accurate to predict the result. Genetic algorithm (GA) optimization was used to determine optimal parameter combinations, and confirmation tests predicted optimised parameters. ANN-GA is effective for optimising welding settings.

S. Mondal et al. [46] found that welding current, gas flow rate, and welding speed affect Duplex Stainless Steel (DSS) weld joints. Controlling these process parameters improves DSS weld junctions. TIG welding process parameters are optimised using Principal Component Analysis (PAC) and Taguchi's signal to noise (S/N). The output response is the weld joint tensile strength, and the optimal parameters are 80 Amp welding current, 7 l/min gas flow rate, and 2.3 mm/sec welding speed. ANOVA determines each factor's impact on output. Extra tests confirm the best

result. PAC enhances weld quality in chemical industries, oil & gas refineries, manufacturing industries, etc.

J. Mirapeix et al. [47] Classified arc-welding errors using a unique approach. Analyzing the plasma spectra created during welding can assess the weld quality. 1 mm AISI 304 stainless steel plates were welded with a 1 mm tungsten electrode, 2 mm root gas, and 12 L/min shielding gas. Principal Component Analysis (PAC) and neural networks are used to discover defects (ANN). Plasma spectral data is processed with a training set to automatically find weld defects. Reducing gas flow and welding current produces penetration problems. Low gas flow or welding current reduces penetration.

Prashant S Lugade et al. [48] concentrated on increasing welding penetration and minimising weld bead width. SiO2 flux with acetone is used to weld 6 mm 304L plates for the experiment, which is designed on the basis of Taguchi's L9 orthogonal array to optimise the process parameters. The electrode gap, welding current, welding speed, and gas flow rate were chosen as the process parameters to be optimised for the desired output response of ultimate tensile strength. The opium production process was optimised by Taguchi to use a 1 mm electrode gap, a 200 A welding current, a 100 mm/min welding speed, and a 10 liters/minute gas flow. ANOVA shows that welding speed (44.87 percent), welding current (28.14 percent), arc gap (20.85 percent), and gas flow rate contribute to tensile strength. (6.12 percent).

S. Omprakasam et al. [49] applied Taguchi's methodology to optimise TIG-welded AA 5052 process parameters and penetration depth. Current, voltage, and speed are used to build an L27 orthogonal array experiment. To optimise process parameters, analysts used ANOVA, SNR, and regression. Regression study demonstrates that the model can predict RFF, PSF, and weld hardness. Taguchi's technique results show a maximum hardness of 145.3 HV 0.5 for RFF 4.49 and PFF 3.83 at 140 A, 18 V, and 300 mm/min. RFF jumps from 40 to 140 A. Current has a greater impact on RFF, PSF, and hardness than voltage and speed, according to S/N and ANOVA.

E. Ahmadi et al. [50] studied the influence of welding settings on penetration and weld bead shape with activated flux. Taguchi's approach with L9 (34) orthogonal array is used to design the experiment and analyse mechanical properties of the welds. Activated flux promotes TIG welding penetration while reducing weld bead width. Taguchi's experimental research demonstrates that welding speed and current are the most effective welding parameters for increasing D/W ratio.

Increasing current and slowing welding increases penetration. Activated flux enhances weld characteristics by reducing HAZ grain size.

Mohamed Farid Benlamnouar et al. [51] employed Taguchi's experimental strategy to optimise the mechanical properties of dissimilar welded joints of X70 and 304L. The experiment is designed using Taguchi's L9 orthogonal array with current, welding speed, gas flow rate, and microstructural and mechanical qualities as output responses. Optical microscopy, SEM microscopy, EDX analysis, and mechanical testing are used to characterise welding parameters, microstructures, and mechanical behaviour. Hardness is linked to microstructural change, not tensile strength. 95% confidence ANOVA analysis. Process parameters should be 70 m/min, 70 A, and 8 lit/min.

D.S. Nagesh et al. [52] used ANN to forecast weld bead geometry and GA to improve welding parameters. TIG welding of 1.6 mm thick 1100 aluminium plate using AWSA5-10 filler rod. Input process parameters are welding speed, filler wire feed speed, cleaning, and root gap. Output response is front and back weld bead height and width. Several leniar regression techniques are utilised to create mathematical models for TIG weld bead shape parameters.

Shamith L Saldanha et al. [53] studied the various aspects of TIG welding and presented it in this paper. TIG welding has different process parameters like welding current, welding speed, wire feed speed, arc length, and shielding gas flow rate that affect weld quality. Controlling them to predict the output is useful in automation processes in industry. Artificial neural networks (ANN) are used to forecast and improve weld bead geometry and input process parameters. ANN is ideal for non-linear and multi-variate data processing. Experimental data is utilised to train feed-forward neural networks using back propagation. ANN's memorization and generalisation errors are low after training and testing in MATLAB.

Daniel Bacioiu et al. [54] employed an HDR camera to assess TIG welding using artificial neural networks (ANN) by image processing. This analysis includes creating a CNN and FCN model by altering internal architecture and hyper-parameters to represent dataset's probability distribution. Here's a critical analysis of the faults associated to input image fidelity reduction, emphasising the drop in accuracy. This analysis checks 33,254 pictures and identifies 5 welding faults.

According to I. Owunna and A-E.Ikpe [55], a central composite design (CCD) was used to develop an experiment to evaluate mechanical properties for 20 samples of TIG-welded AISI

4130 Low carbon steel plate. The best 20 samples are selected by ANN. The predicted and measured values are very close. UTS of 421 MPa, modulus of elasticity of 793 MPa, strain 0.61 and elongation of 61 percent were anticipated by the algorithm ANN optimization. A UTS of 427 MPa, a modulus of elasticity of 806 MPa, a strain of 0.62, and an elongation of 62% were obtained utilising optimised input variables in the experiments. SEM/EDS shows that the grain sizes of iron, chromium, molybdenum, and nickel in the weldment are uniformly distributed across the weld (Ni). ANN software can be used to provide accurate and trustworthy results in order to save time and resources..

Rohit Kshirsagar et al. [56] employed ANNs to estimate TIG weld bead geometry from input parameters. For tiny data sets, ANNs have only one hidden layer, which affects accuracy. ANNs can't capture rapid shifts in input–output trends, such a wide range of heat inputs resulting in a flat crown (zero crown height). Support vector machine (SVM) and ANN can tackle this problem. SVM covers several input parameters.

1.9 SCOPE AND OBJECT OF PRESENT WORK

With this information, it is clear that a wide range of quality elements of the weldment can be directly or indirectly affected by a variety of process control factors, such as welding current, voltage and gas flow rate in TIG welding (commonly known as TIG welding). Input parameters such as current, voltage, electrode stick-out, gas flow rate, edge preparation, welding position, and welding speed are all expected to have a significant impact on weld quality, which is well-known to be dependent on bead geometry and mechanical-metallurgical characteristics of the weld. More importantly for welds in actual use, these quality indices establish how much joint strength is required to meet the functional requirements of a particular weld. As a result, the task of preparing a high-quality weld appears to be a difficult one. Research into the impact of these parameters on weld bead geometry and microstructure, as well as other elements of TIG welding, has been done to some extent, according to a review of the published literature. The type of filler metal used can have an impact on the final weldment's quality, among other things. As a result of a literature

review, it was discovered that weld mechanical and metallurgical features have not been thoroughly studied. Stainless austenitic steel welding, and TIG welding in particular, is one of the areas where more thorough study contributes in a significant way to the exact control of welding method for improved and acceptable weldment quality. In order to have a deeper understanding of the many facets of TIG welding, more study is required. Experimentation and analytical study and modelling can be used to examine the impact of process parameters on different outcomes. Modeling process responses using multiple linear regression and response surface methods can be done with a variety of tools. In order to find the most effective configuration of the parameters, each quality feature is optimized (maximized or minimized) in accordance with the demand. This strategy, on the other hand, can be used to improve a single goal function. When dealing with many objectives, it is vital to turn them into a single objective function that must be optimized at the end of the process. Many studies have found the Taguchi approach to be effective. OA design and the concept of quadratic quality of responses are used in conjunction with a small number of well-balanced tests to arrive at this method's conclusions. A multi-objective optimization problem cannot be solved using the usual Taguchi approach. Grey relational analysis and the Taguchi method will be used to combat this.

There has been a lot of research done on many elements of welding, but there is still need for more research into the impact of different processes/input parameters on the quality of weld in austenitic stainless steels when using TIG welding. TIG welding of austenitic stainless steels has a wide range of input parameters/features that can affect the quality of the weldment. Besides current, gas flow rate, voltage, welding speed, electrode stick-out, the type of inert gas or gas mixture, there are other input features also. Filler rod diameter and composition, power source parameters, welding position, etc. are all factors to consider when preparing the edge for welding. The effect of these characteristics or variables on the quality of the weld will require a great deal of investigation. TIG welding of austenitic steel necessitates extensive experimentation, analysis and modelling in order to gain a better knowledge of the phenomena, control parameters, parametric optimization of the process, and forecast and regulate desired responses (quality indices). As a result of numerous investigations, a knowledge base can be built that can be used by engineers and technicians in the field to perform high-quality welds with more precision, reliability, and foresight.

Keeping this in mind, some of the input characteristics have been taken into account in this study in order to determine how these parameters affect the quality of the weld. TIG welding of 3mm thick austenitic stainless steel uses these parameters: current and gas flow rate. Butt welded joints' ultimate strength and breaking strength in tensile load are examined responses. Additionally, the impact of varying the filler material composition has been taken into account. As a result, the current, gas flow rate, and filler material used in austenitic stainless steel TIG welding will be studied in this research. In addition to the answers in terms of ultimate and breaking strengths, optical and X-ray radiographic tests have also analysed the levels of flaws like porosity, lack of fusion, undercut, etc. Additionally, microstructural studies have been carried out. Using experimental data, regression analysis and Taguchi-based grey relational analysis can now be used to examine the data. Predicting responses to varying current and gas flow rates has also been done mathematically. Grey-based Taguchi approach was used to solve the optimization problem in order to determine the best parametric combination for the desired weld quality. As a result, certain important conclusions can be taken from both experimental results and the analysis of data.

CHAPTER 2

EXPERIMENTAL PLAN, SET-UP AND PROCEDURE

2.1 INTRODUCTION

TIG welding was used in this study to examine the effect of process parameters on the ultimate tensile strength and % elongation of austenitic stainless steel butt welded joints. Additionally, process improvement has been attempted. Welding the butt was done using stainless steel of 3 mm thickness. The following sections detail an experimental TIG welding setup and method.

2.2 EXPERIMENTAL PLAN

It has been used to plan the welding experiments of austenitic stainless steel, as stated in the preceding chapter. The L9 orthogonal array was chosen by taking into account three variables, each with three levels. Current, gas flow rate, and arc gap are all taken into account as input parameters in this study. Samples were made utilising varying levels of current, gas flow rate, and arc gap for nine distinct butt welds. The levels of the factors are determined by doing trial runs and conducting a literature review. Table 2.1 lists the variables and their corresponding concentrations utilised in the experiments. It is listed in Table 2.2 the welding settings that have been almost identical in all nine experiments. The experimental design matrix for each factors are shown in Table 2.3.

Table 2.1: Process parameters and their levels

Process Parameters	Symbols	Unit	Level 1	Level 2	Level 3
Welding Current	C	Ampere (A)	**90**	**100**	**110**
Gas flow rate	G	liter/min	**10**	**15**	**20**
Arc gap	A	mm	**2**	**3**	**4**

Table 2.2: Fixed welding conditions

Polarity	AC (alternating current)
Arc Voltage	25 V
Electrode Diameter	2.4 mm
Root gap	2 mm
Shielding gas	Argon (99.99%)

Table 2.3: Experimental design matrix as per L9 orthogonal array

Sample No.	Current	Gas flow rate	Arc gap
S1	90	10	2
S2	90	15	3
S3	90	20	4
S4	100	10	3
S5	100	15	4
S6	100	20	2
S7	110	10	4
S8	110	15	2
S9	110	20	3

Table 2.1 specifies how butt welded joints are constructed. A preliminary experiment of this nature has been carried out thus far. Welded samples were to be examined by visual examination, X-ray radiography tests, tensile tests, hardness tests, and microstructural studies were next on the agenda.

2.3 EXPERIMENTAL SET-UP

In this part, the equipment used in the current project is described. The base material and filler rod specifications are also included. Procedures are detailed in Section 2.3.

2.3.1 EQUIPMENT AND INSTRUMENTS USED

The main set-up of the experiments includes the TIG welding machine.

Welding machine

The experiments have been performed on Tungsten Inert Gas Welding Machine (Make: Weldman Synergic Pvt. Ltd., India). The photographic views of this setup are shown in the Figure 2.1

A) SPECIFICATIONS OF TIG MACHINE:

a) MAKE	**:** Weldman Synergic Pvt. Ltd.
Type	: THYRISTORISED
b) POWER SUPPLY UNIT:	
Rated input	**:** 415V/ 3PH/ 50Hz
Input current (at 60% Duty cycle)	: 22.5A
O.C.V	: 85 V
Max.welding current (at 60% Duty cycle)	: 300A
Min. welding current	: 10A
Type of cooling	: AB
Class of insulation	: H
Max. Continuous automatic welding current	: 210A
Weight (approx)	: 305 kg.

d) TORCH:

Type	: TTA-200 Straight neck
Welding	: Manual

e) GAS REGULATOR:

Make : IOL ltd.(India)

Type : ARGON IAR-58

Figure 2.1 Tungsten inert gas welding machine used in the work

X-ray radiography machine

X-ray radiography tests have been done at SKB metallurgical services, Salkia, Howrah-111062. The important specifications of this equipment are shown in Table 2.4.

Table 2.4: Specifications of the X-ray radiography machine

Source	X-ray
Equipment details	XXQ-2005
Voltage	120 kV
Current	5 mV
Film	LASER NDT-7
Sensitivity	< 2%
SOD	28”

Screen	0.15 mm(both)
Technique	S.W.S.I.
IQI	ASTM-1A
Exposure time	30 Sec
Processing temperature	20^0C

Milling machine

Milling machine is used toprepare micro hardness and tensile sample by cutting required amount of strip from the welded sample. The specification of the milling machine is given in the Table 2.5 and photographic view of the Milling machine used in the work is shown in Figure 2.2.

Table 2.5: Specifications of the Milling machine

Type	Universal Milling Machine
Maker Name	B. S. Machine Tools Corporation
Serial Number	222484

Figure 2.2 Milling machine used in the work

Instron universal testing machine

An Instron universal testing machine has been used to conduct tensile tests at Jadavpur University's Fatigue fracture damage analysis (FFDA) laboratory. Using a hydraulic chuck, as shown in Figure 2.3, specimens are held in place. A summary of the machine's primary characteristics may be found in Table 2.6. Additionally, an image of the machine is shown (Figure 2.2).

Table 2.6 Specification of Instron universal testing machine

Model number	5582
Serial number	95/1058
Maximum capacity	600 KN
Maximum temperature	1000^0C

Figure 2.3 Photographic view of Instron universal testing machine

Metallurgical microscope

In the present work, Leica metallurgical microscope is used for study of the microstructures of the welded samples. The major specifications are given in Table 2.7. A photographic view of metallurgical microscope is shown in Figure 2.4.

Table 2.7: Specification of the metallurgical microscope

Model number	DMILM
Focusing	3 gear focusing
Incident light	sturdy incident light axis with 4x and 5x reflector turrets
Transmitted light	12 V, 100 W halogen
Power supply	90-250 for 12 V 100 W, frequency 50-60 Hz

Figure 2.4 Photographic view of the Leica metallurgical microscope

Micro-hardness tester

This instrument has been used to measure hardness at different regions of the weldment. This has been a UHLVMHT MOTmicro-hardness tester, shown in Figure 2.5. Some important specifications are given in Table 2.8.

Table 2.8: Specification of micro-hardness tester

Model number	VMH-002V/1903001
Software	IMS-VHMT
Zoom	10x – 50x

Indentation load	10gf – 2000gf

Figure 2.5 Photographic view of the Leco LM 248AT micro-hardness tester

2.3.2 COMPOSITION OF THE BASE MATERIAL AND FILLER WIRE

The tungsten inert gas welding procedure is used to weld austenitic stainless steel sheet in this thesis. The specimens are 100 x 60 x 3 mm in size. The samples were cut with a shear cutter without any particular preparation of the edges. The tungsten filler has a diameter of 2 mm. Tables 2.9 show the compositions of the base material and the filler wire, respectively.

Tables 2.9 show the compositions of the base material and the filler wire

	C	Mn	Si	S	P	Cr	Ni	Mo	Fe
Base Metal (AISI304L)	0.028	1.52	0.60	0.02	0.040	18.45	8.12	0.05	Bal.
Filler Metal (ER308L)	0.030	1.54	0.65	0.030	0.045	19.20	8.68	0.02	Bal.

2.4 EXPERIMENTAL PROCEDURE

AISI 304L austenitic stainless steel was used in this thesis project. There are a total of eighteen welding samples, each measuring 100 mm by 60 mm by 3 mm. Using a fixture, the welding set-up has been prepared and tested to ensure it is ready for use. Two sample pieces are welded together to form butt joints. Using Taguchi's orthogonal array design of experiments, a total of nine welded samples were created by conducting welding at various levels of current, gas flow rate, and arc gap. Figures 2.6 to 2.14 provide a photographic view of the all welded specimen.

Fig 2.6 Photographic view of sample number 1

Figure 2.7 Photographic view of sample number 2

Figure 2.8 Photographic view of sample number 3

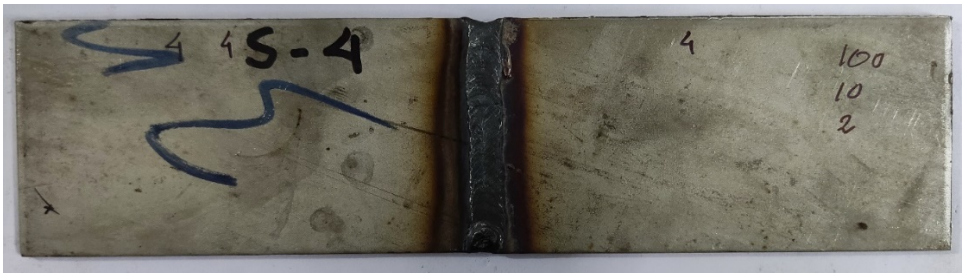

Figure 2.9 Photographic view of sample number 4

Figure 2.10 Photographic view of sample number 5

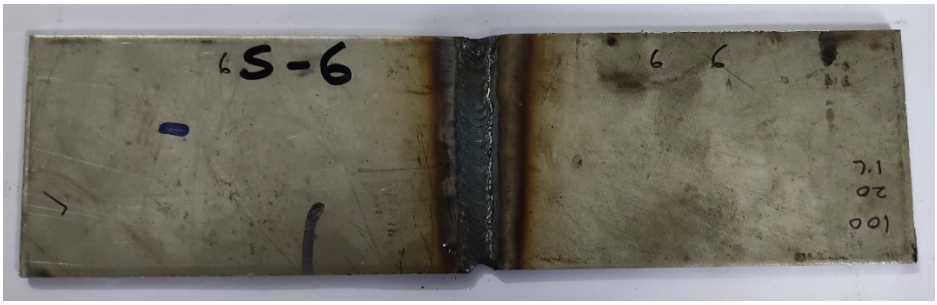

Figure 2.11 Photographic view of sample number 6

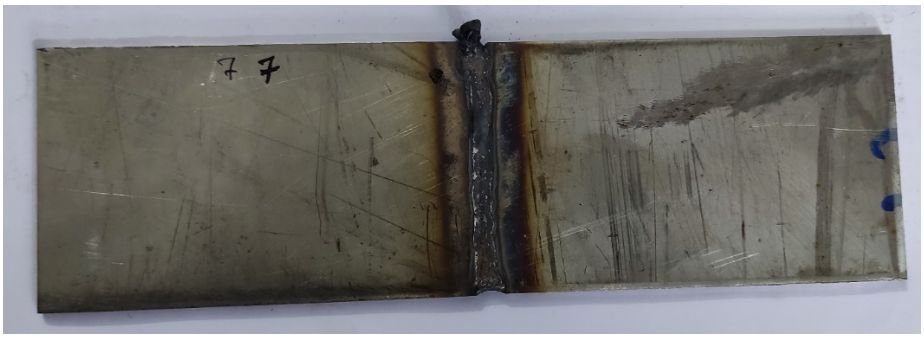

Figure 2.12 Photographic view of sample number 7

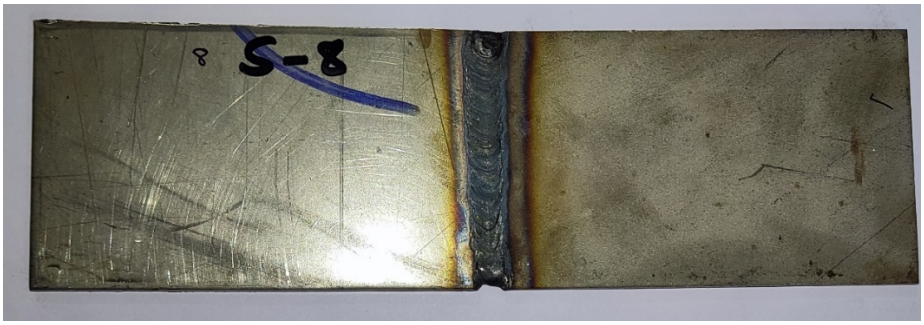

Figure 2.13 Photographic view of sample number 8

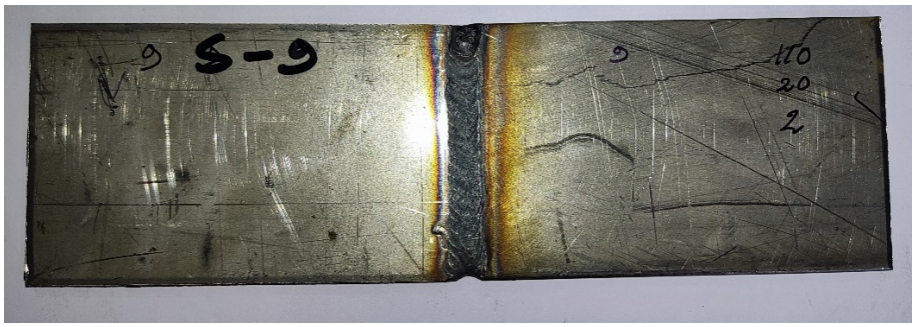

Figure 2.14 Photographic view of sample number 9

A visual evaluation of nine samples was conducted after the welding samples were simply cleaned. All of the welded samples are subjected to X-ray radiography. In the milling machine, tensile test samples were cut from the weld strip using a cutter.

Figures 2.15 to 2.23 depict a photographic view of a tensile test specimen.

Figure 2.15 Photographic view of the tensile test specimen number 1

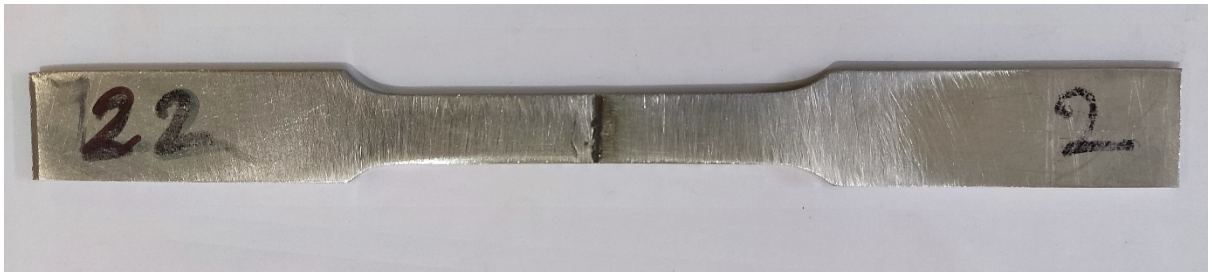

Figure 2.16 Photographic view of the tensile test specimen number 2

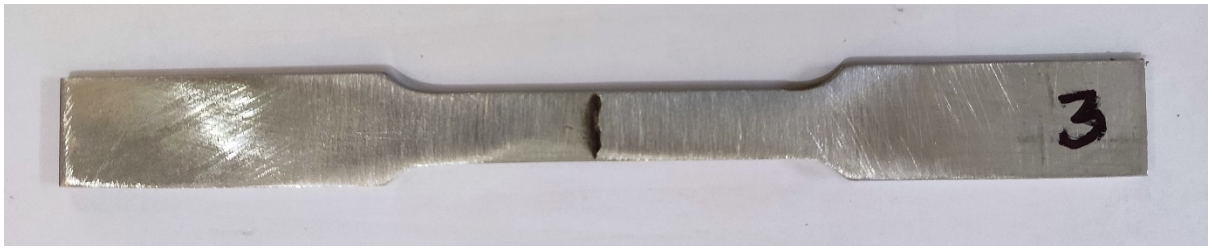

Figure 2.17 Photographic view of the tensile test specimen number 3

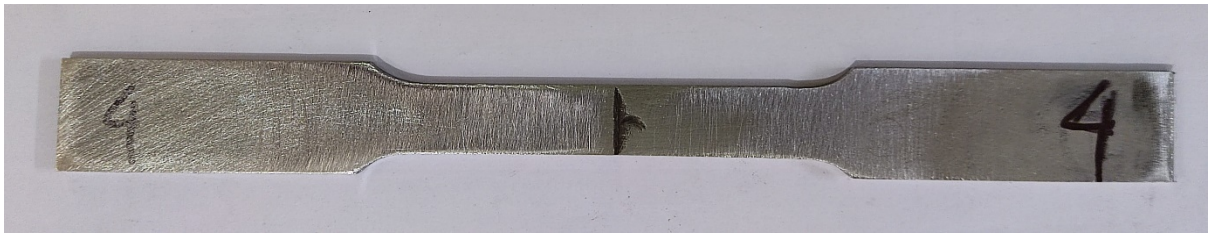

Figure 2.18 Photographic view of the tensile test specimen number 4

Figure 2.19 Photographic view of the tensile test specimen number 5

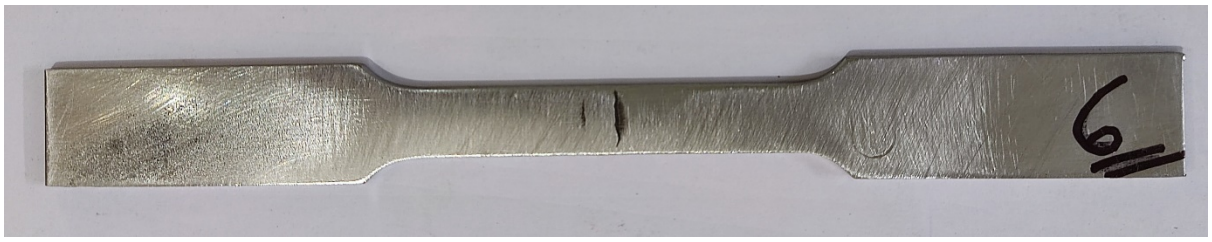

Figure 2.20 Photographic view of the tensile test specimen number 6

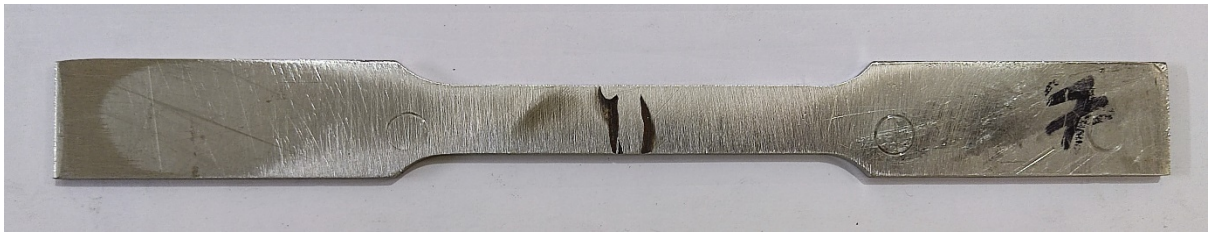

Figure 2.21 Photographic view of the tensile test specimen number 7

Figure 2.22 Photographic view of the tensile test specimen number 8

Figure 2.23 Photographic view of the tensile test specimen number 9

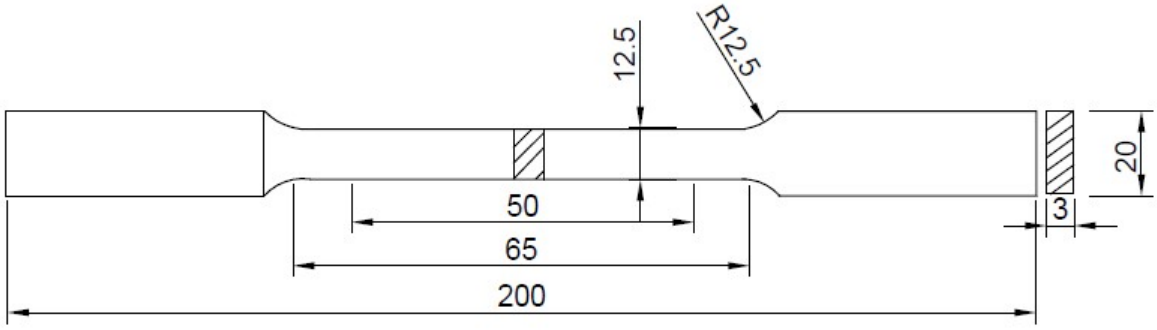

Figure 2.24 shows the dimensions of the tensile test specimens

This machine, which is housed in the Mechanical Engineering Department, Jadavpur University's FFDA Laboratory, performs tensile tests on the specimens and observations are made. Figure 2.24 shows the dimensions of the tensile test specimens. The samples are held in place by a hydraulic jaw during the testing process. Microstructural analysis is performed on a tiny fraction of the specimens during the fabrication of the tensile test specimen. Finally, the middle component of each of these cut-out pieces has been removed and prepared for microstructural analysis.

Samples for microstructural research have been ground, polished, and finally etched. It is etched using aqua regia (3HCl + 1 HNO3) solution. Samples of base metal, heat affected zone (HAZ), and weld metal have been examined under a Leica microscope; images have been taken. Additionally, a microhardness test has been performed on each of these samples. During this process, the hardness of the weld metal, the high-hazard zone, and the base metal were all measured. Previously, the Leco microhardness tester was mentioned.

CHAPTER 3

RESULTS AND DISCUSSION

3.1 INTRODUCTION

After Experimental plan, set up and procedure followed to complete the experiments, some results are obtained and are shown in this chapter. In order to identify the optimal parametric combination for the desired weld quality, an optimization problem was solved using the Grey-based Taguchi method in this section of the work.

3.2 RESULTS OF VISUAL INSPECTION AND DISCUSSION

After welding was complete, all of the samples were visually inspected. Table 3.1 displays the data collected during the experiment. Some of the welded samples have faults that may be recognized visually, such as undercutting along the welding line and a lack of fusion on the other side of the join. In some examples, such as samples 1 and 6, nearly no faults are discovered under specific parametric settings. Errors in some samples can be the result of environmental factors such as voltage fluctuations, semi-automatic machine setup, and others. The welder's competence is critical to the quality of the weld, as the operation is done manually and human error can readily impair the weld development. Weld flaws can be caused by imperfections or in homogeneities in the base metal plates and filler wire.

Table 3.1: Results of visual inspection

Sample number	Sample identity	Observation
1	S1	No defect
2	S2	Incomplete Penetration
3	S3	Incomplete Penetration
4	S4	No defect
5	S5	Excessive deposition
6	S6	No defect
7	S7	No defect
8	S8	No defect
9	S9	Undercut, Excessive deposition

Austenitic stainless steel weld samples are visually inspected for surface flaws after welding. Visual inspection is the only approach to verify a large number of welds. This is the most popular method for examining weldments due to its simplicity, speed, and cost-effectiveness. Table 3.1 reports visual inspection results. This table shows that no defects were identified for specified welding conditions. These are for S1, S4, S6, S7, and S8. One or more other samples exhibited blow holes, spatter, and undercutting. Low or high current and/or transit speed may have caused blow holes. Incorrect welding method, stringer or weaved beads, filthy job surface, and damp filler rod may cause blow holes or porosity. Blow holes and porosity may have been caused by gas trapped in hardening metal, a stronger arc, etc. Incorrect welding current, gas flow rate, and nozzle-to-plate distance can cause undercuts. Higher arc travel speed or longer arcs, and improper filler rod might cause undercut. The next section covers the potential reasons of the sample and X-ray radiography abnormalities.

3.3 RESULTS OF X-RAY RADIOGRAPHY TEST AND DISCUSSION

X-ray radiography tests have been done for all the welding samples after the visual inspection. The results are shown in the Table 3.2.

Table 3.2: Results of X-ray radiography test

Sample number	Sample identity	Observation
1	S1	No defect
2	S2	Porosity, Lack of Fusion
3	S3	Porosity, Lack of Fusion
4	S4	No defect
5	S5	Lack of Fusion
6	S6	No defect
7	S7	No defect
8	S8	No defect
9	S9	Porosity, Lack of Fusion

The results show that most of the samples possess enough significant defects. Under the corresponding welding conditions, defect-free joints have been obtained (sample numbers 1-8).The X-ray Radiography diagrams are shown in Figures 3.1-3.9.

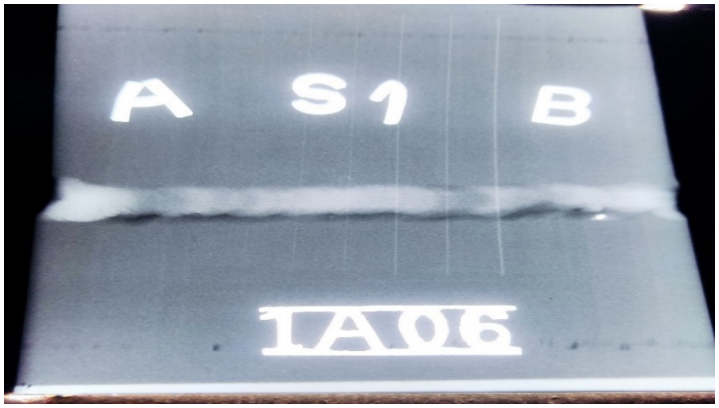

Figure 3.1 X-ray Radiography film for sample S1

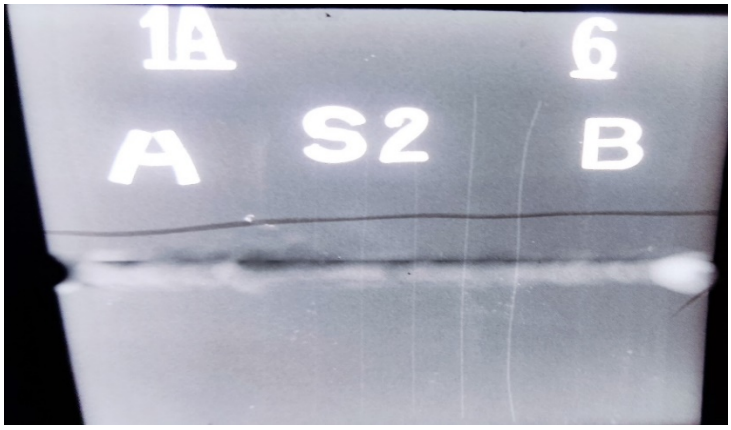

Figure 3.2 X-ray Radiography film for sample S2

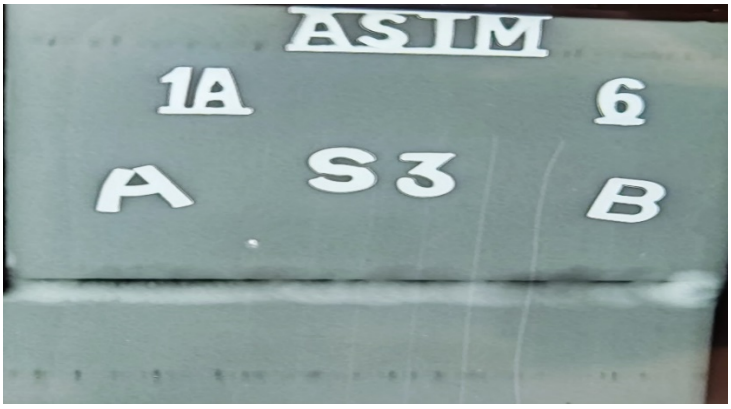

Figure 3.3 X-ray Radiography film for sample S3

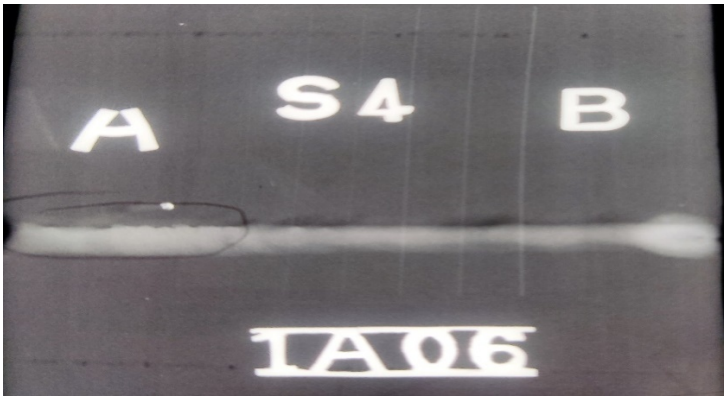

Figure 3.4 X-ray Radiography film for sample S4

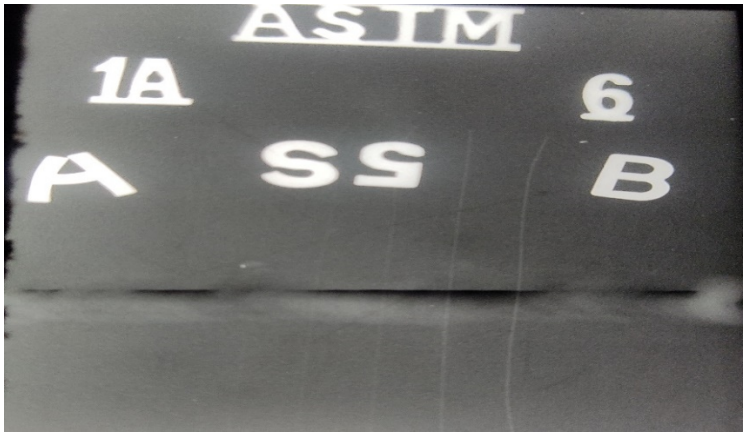

Figure 3.5 X-ray Radiography film for sample S5

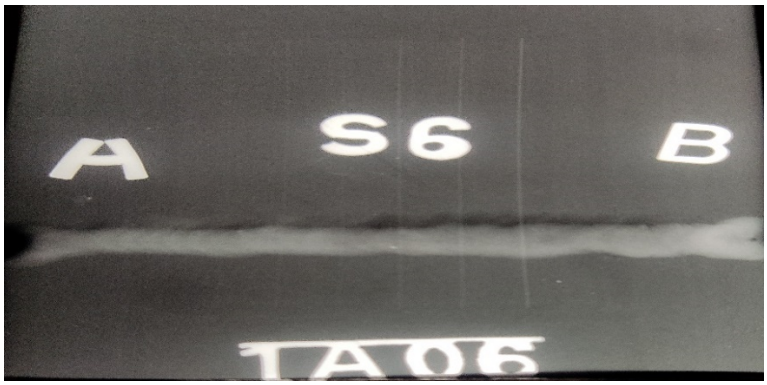

Figure 3.6 X-ray Radiography film for sample S6

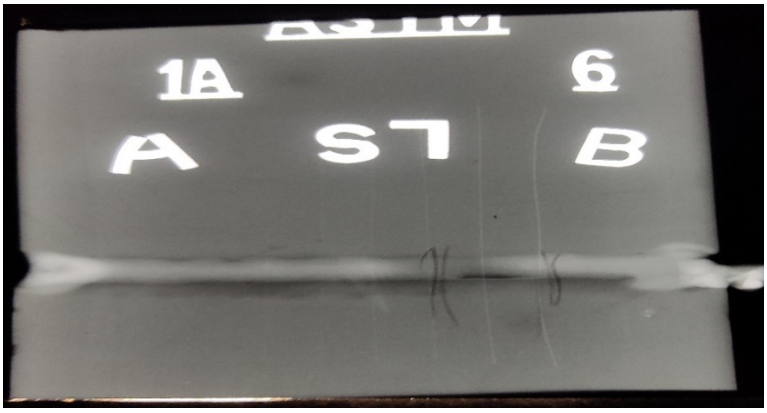

Figure 3.7 X-ray Radiography film for sample S7

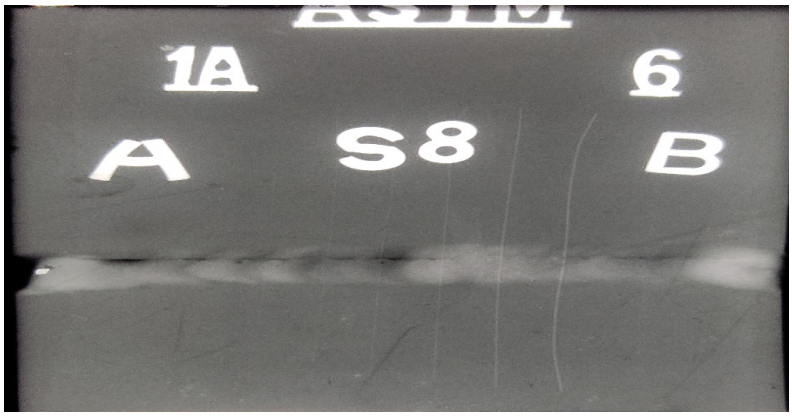

Figure 3.8 X-ray Radiography film for sample S8

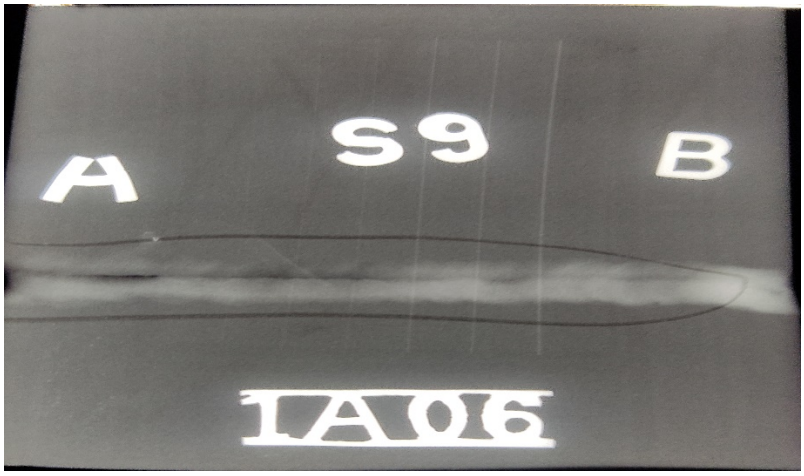

Figure 3.9 X-ray Radiography film for sample S9

The X-ray defect detector XXQ-2005 was used to conduct X-ray radiography testing on all 20 welded samples after the visual examination was completed. Table 4.2 summarizes the findings in this study. Figures 3.1 –3.9 depict the photographic views of the X-ray films.

It is possible that the deposited metal did not fuse effectively with the base metal because of poor setup of the current or improper cleaning, quicker arc travel speed, or the presence of oxides, scale, and other contaminants. The weld deposit will not melt properly if the heat input is too low. A possible explanation for the presence of porosity in samples S2, S3, and S9 is gas entrapment during solidification. Porosity can be a serious issue that is difficult to fix.

3.4 RESULTS OF TENSILE TEST AND DISCUSSION

Tensile test has been performed on Instron machine, to examine the regions from where failure/fracture has occurred and to find important mechanical properties of the welded samples. The results of tensile tests are given in Table 3.3.

Table 3.3: Tensile test results

Sample number	Sample identity	Yield strength (MPa)	Ultimate Tensile Strength (MPa)	Percentage elongation (%)
BASE PLATE AISI 304L		172.1	589.4	36.2
1	S1	180.1	565.2	30.5
2	S2	149.6	568.2	31.8
3	S3	198.9	430.5	24.4
4	S4	180.0	437.0	20.8
5	S5	197.2	440.0	27.8
6	S6	190.0	450.8	27.6
7	S7	211.5	536.4	21.0
8	S8	190.4	495.4	22.0
9	S9	179.2	432.5	20.2

The data shown in Table 3.3 indicate that for many of the samples, performance of the butt welded joints is satisfactory. For the sample nos. S2 very good ultimate tensile strength is obtained, highest being 568.2 MPa. The highest value of percentage elongation is observed to be 31.8% (for sample no. S2). The lowest value of percentage elongation is exhibited in the sample no. S9 (20.2 %).

Stress-Strain curves, corresponding to tensile test results of all the samples are shown in Figures 3.10–3.19. Typical ductile behavior is observed in almost all the stress – strain curves.

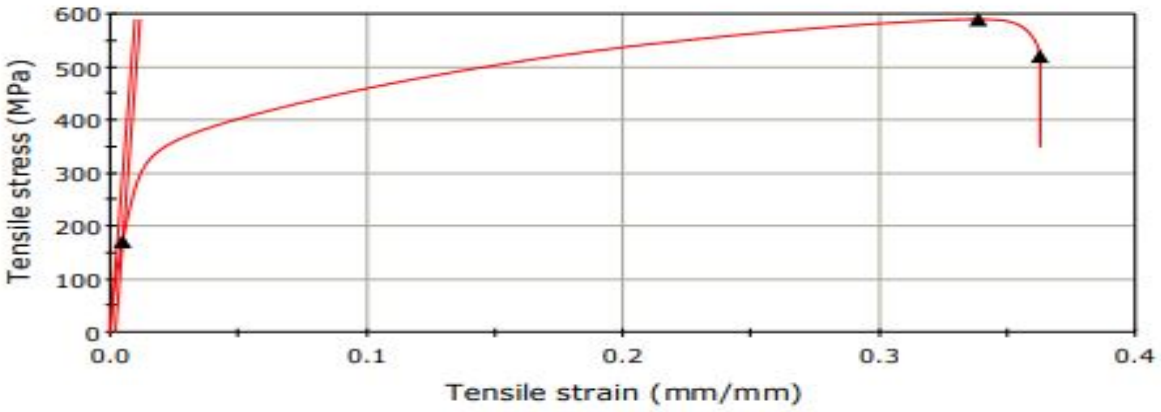

Figure 3.10 Tensile Test Diagram for Base Plate: AISI 304L

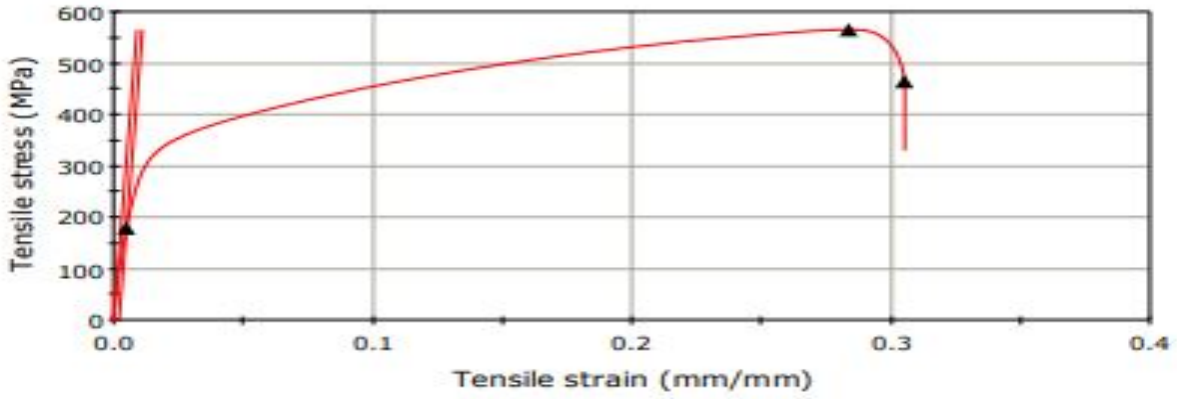

Figure 3.11Tensile Test Diagram for sample S1

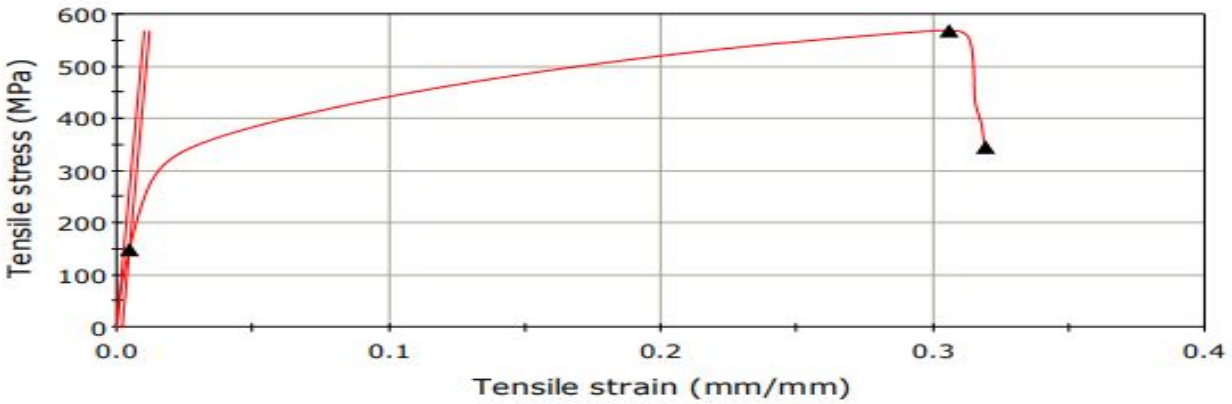

Figure 3.12Tensile Test Diagram for sample S2

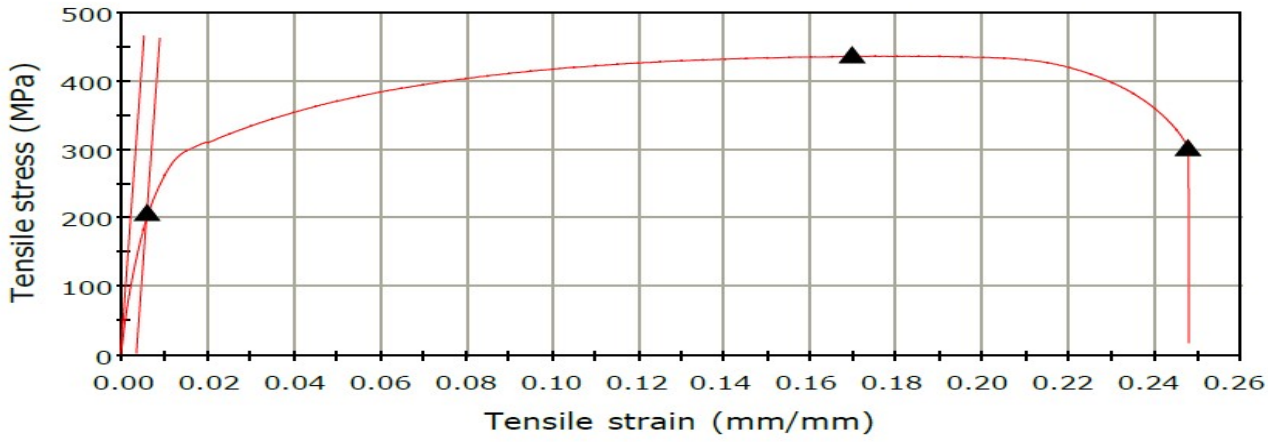

Figure 3.13Tensile Test Diagram for sample S3

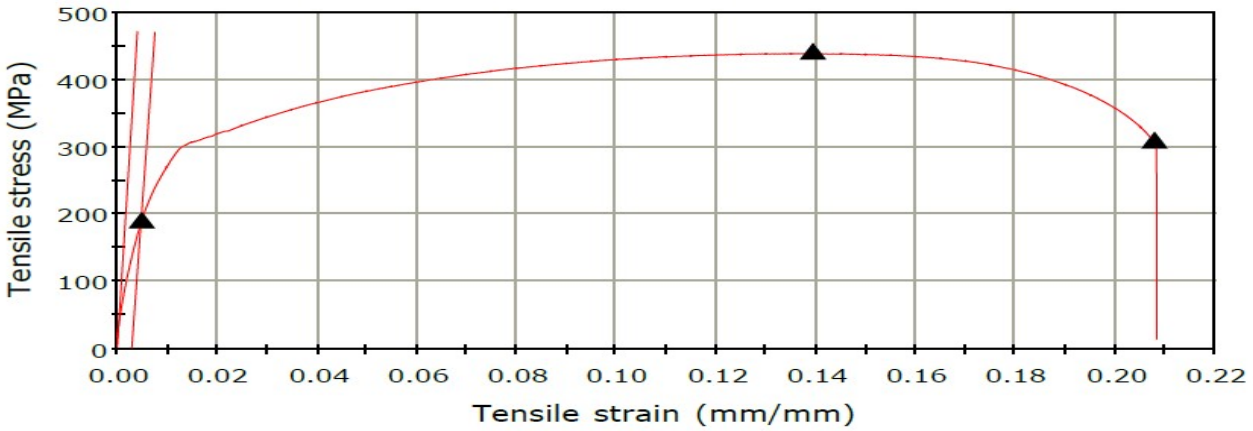

Figure 3.14Tensile Test Diagram for sample S4

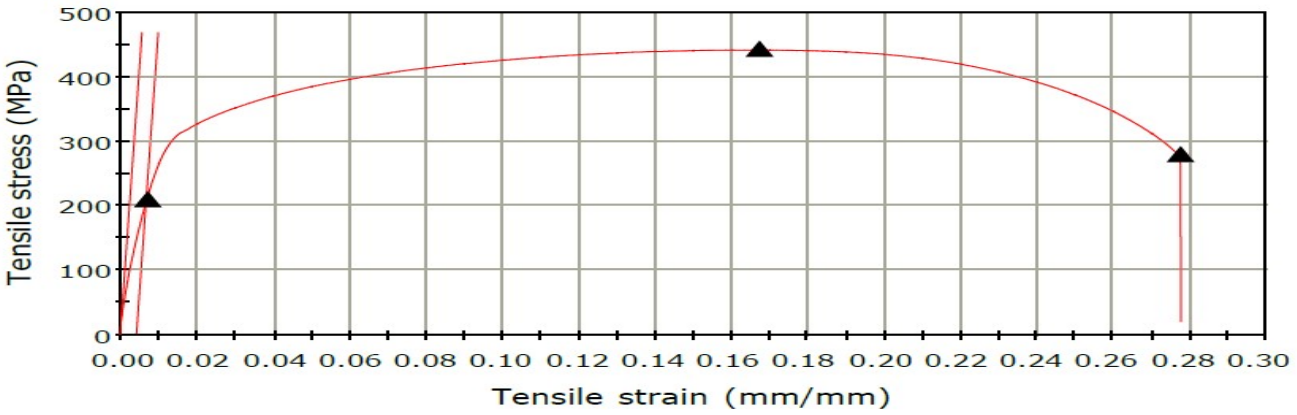

Figure 3.15Tensile Test Diagram for sample S5

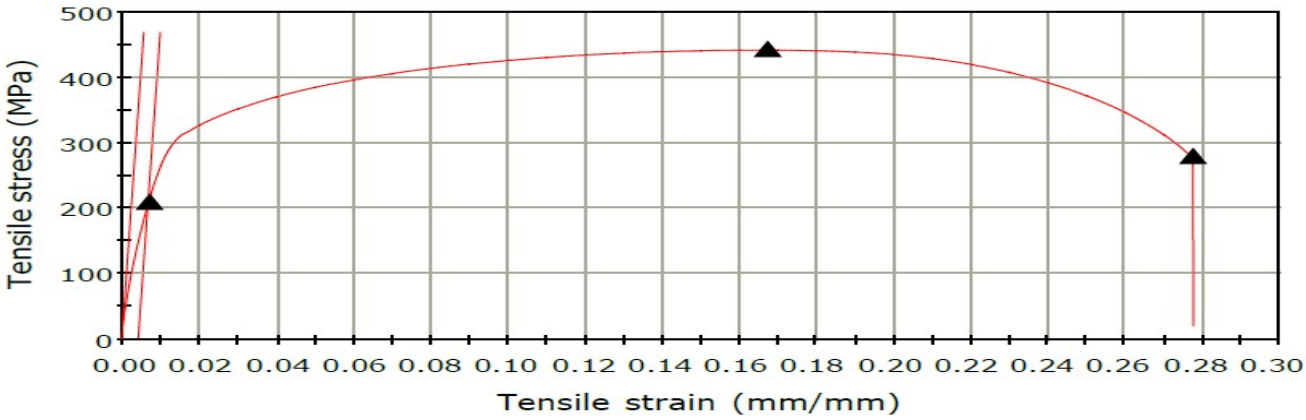

Figure 3.16Tensile Test Diagram for sample S6

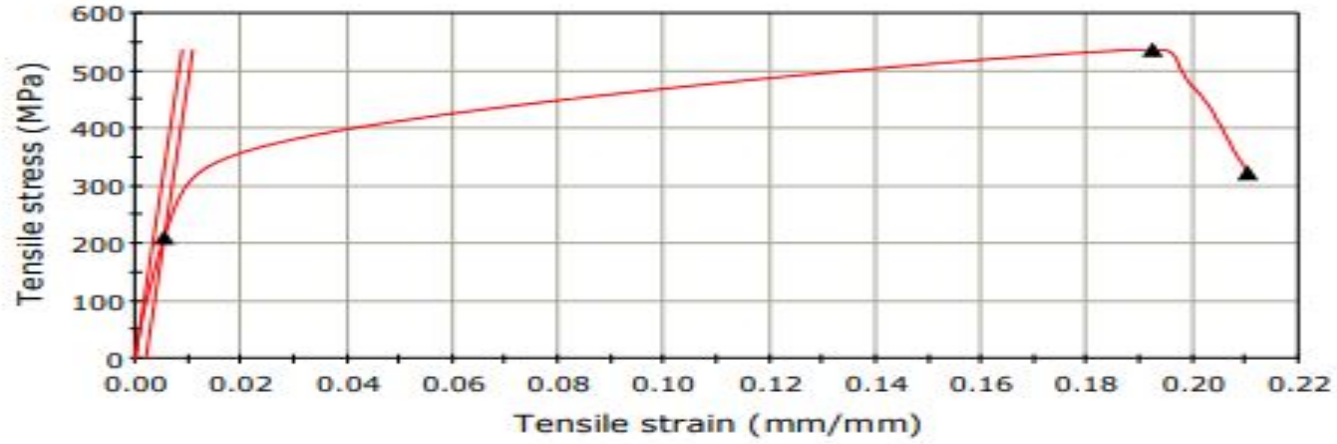

Figure 3.17Tensile Test Diagram for sample S7

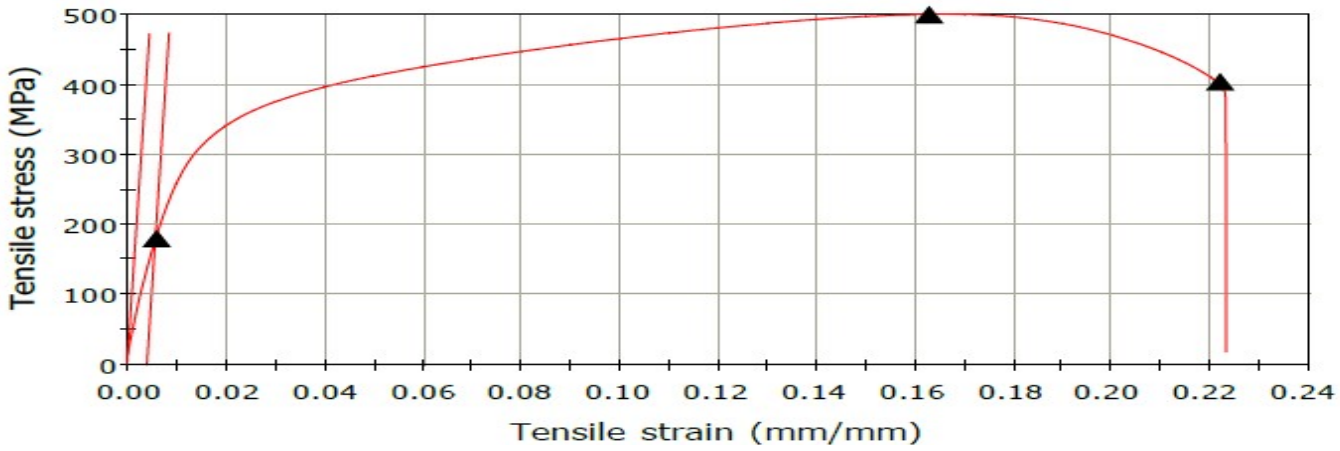

Figure 3.18Tensile Test Diagram for sample S8

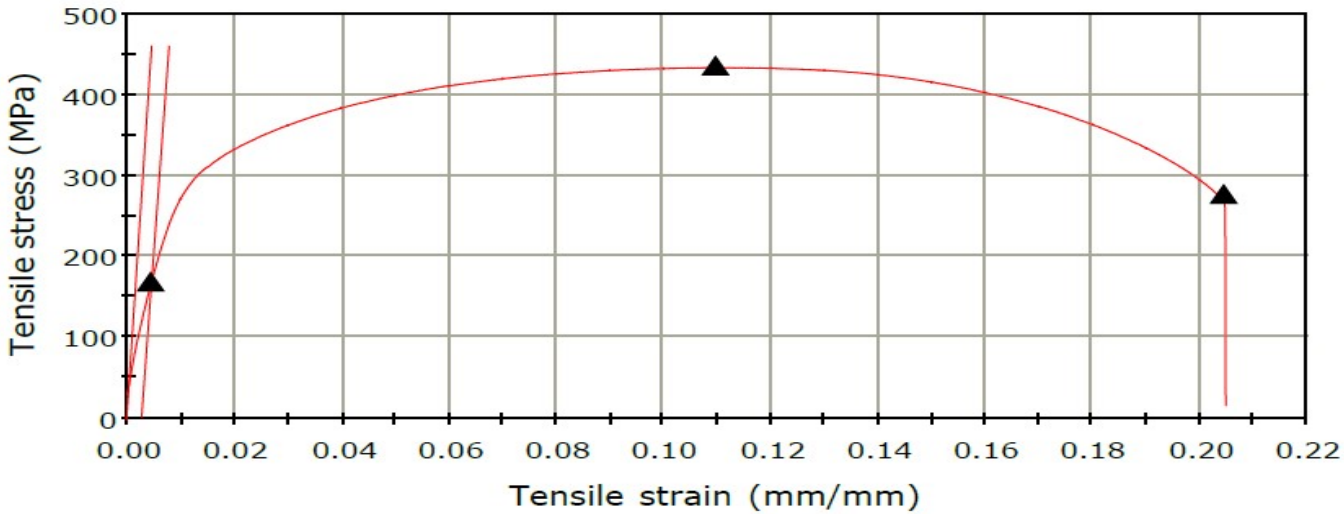

Figure 3.19Tensile Test Diagram for sample S9

3.5 RESULTS OF MICRO-HARDNESS TEST AND DISCUSSION

To measure a material's hardness, one must test its resistance to being indented. Abrasion, scratching, shape, etc. are all common causes of damage. Resistance to wear improves as the hardness of a material increases. However, a material's brittleness increases as its hardness increases. Since various microstructures can be spotted in different zones (weld area, HAZ, and base metal), hardness is a critical attribute for welded joints.

Hardness can be measured in a variety of ways, each of which is based on a specific premise. A Leco LM 248AT micro-hardness tester was used to gauge the hardness of all the samples in this investigation. Six places have been chosen to measure micro hardness values for the purpose of this experiment. Figure 3.20 depicts the position of microhardness. Two spots in the base metal, two points in the HAZ, and two points in the weld zone are measured. Table 3.4 displays the results of the micro hardness test.

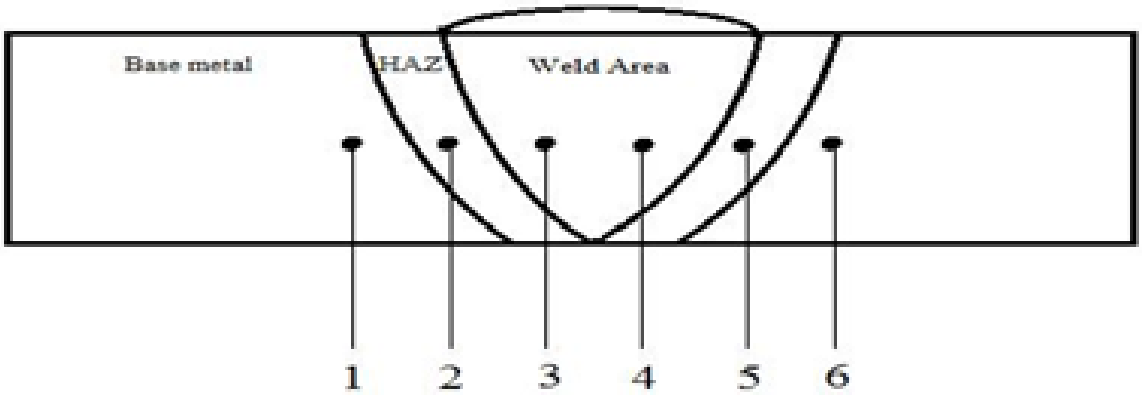

Figure 3.20 Diagram showing positions of hardness measurement

Table 3.4: Results of hardness value

Sample number	Hardness value (HV)					
	Position					
	1 (Base)	2(HAZ)	3 (Weld)	4 (weld)	5 (HAZ)	6 (Base)
1	381	359	428	400	387	414
2	308	317	339	338	283	228
3	312	338	367	363	318	286
4	307	278	294	289	281	266
5	226	286	334	321	259	266
6	292	278	284	304	274	315
7	231	239	257	292	228	218
8	250	268	266	266	264	271
9	295	311	309	331	312	278

Hardness values, in different regions of the welded samples, also indicate the effect of heating and cooling cycles during welding and subsequent cooling of the twenty samples, made under varied conditions of welding. Now, weldment consists of both parent material and electrode material. Compositions of these two materials are not exactly same. Further, heat input rate, cooling rate and many other factors influence the final microstructure of the weld metal. Hardness of weld metal is thus dependent on the development of the type of microstructure developed in the weld region. Variation of weld – metal hardness with respect to base metal, as found from the graphs and data can be attributed to the phenomenon described above. Width of heat affected zone and its characteristics (like hardness etc.) depend upon the temperature upto which this region is heated up during welding, heat input rate and subsequent cooling cycle. All these are influenced by the properties of the base material, the levels of the input parameters etc. As mentioned earlier it is desirable (though difficult) to achieve uniform properties of weld, HAZ and base material. For most of the samples, the nature of variation in hardness values along the position 1 - 2 – 3 – 4 – 5 – 6, is similar. There is slight increase in hardness value within the region HAZ to weld, generally. However, even there are variations in HV values along 1 - 2 – 3 – 4 – 5 - 6, these variations are not very excessive

3.6 STUDY OF MICROSTRUCTURES AND DISCUSSION

Study of microstructures has been made for all the welded samples and the photographs are taken in weld and HAZ regions, for each of the samples. Base metal microstructure has also been studied. The photographic view of base metal microstructure is shown in Figure 3.21 and micro structural view of all the samples are shown in Figure 3.22-3.30.

Figure 3.21 Metallographic view of sample number: BASE METAL 304L

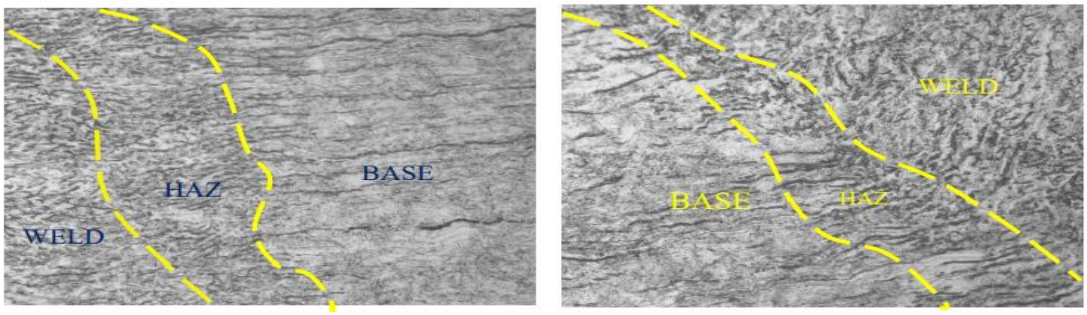

Figure 3.22 Metallographic view of sample number 1

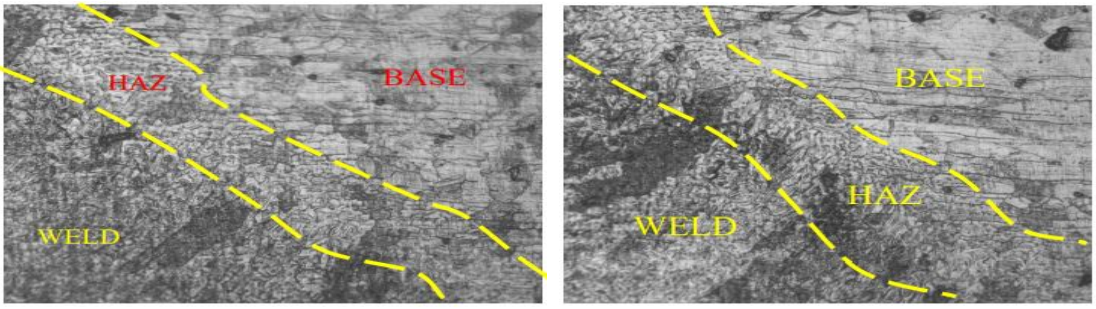

Figure 3.23 Metallographic view of sample number 2

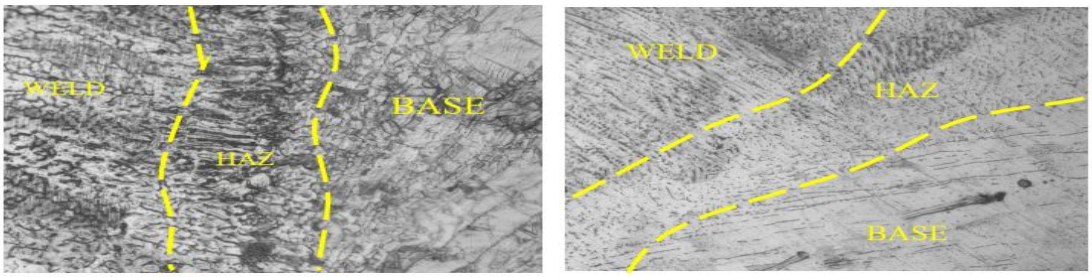

Figure 3.24 Metallographic view of sample number 3

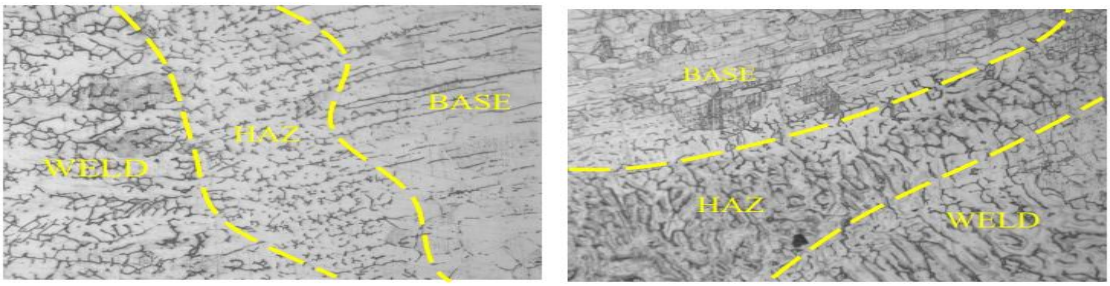

Figure 3.25 Metallographic view of sample number 4

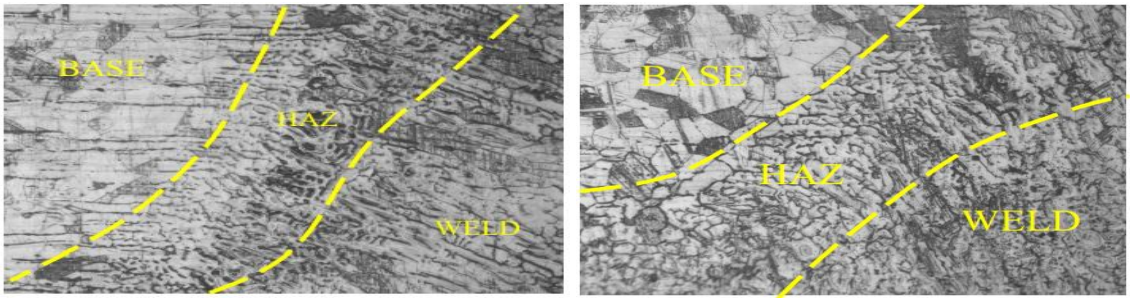

Figure 3.26 Metallographic view of sample number 5

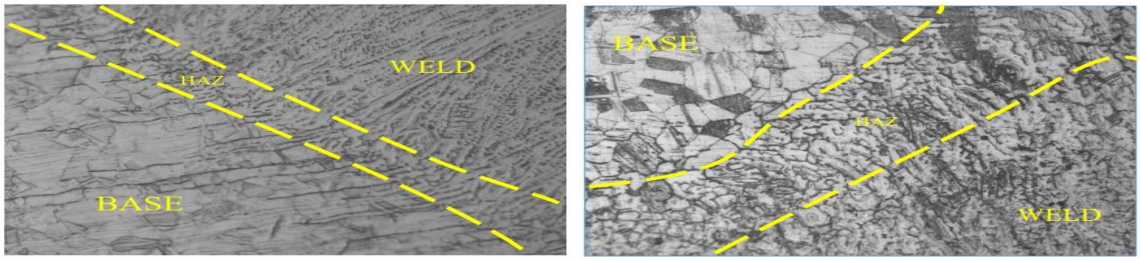

Figure 3.27 Metallographic view of sample number 6

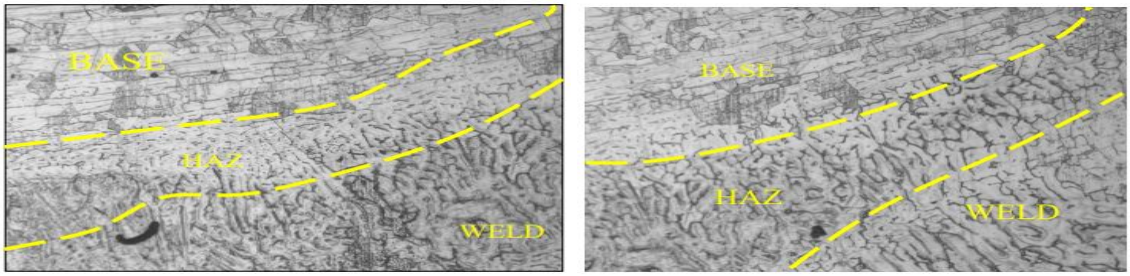

Figure 3.28 Metallographic view of sample number 7

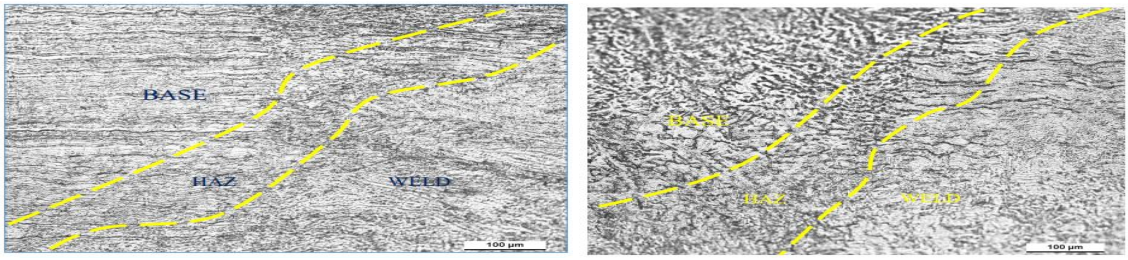

Figure 3.29 Metallographic view of sample number 8

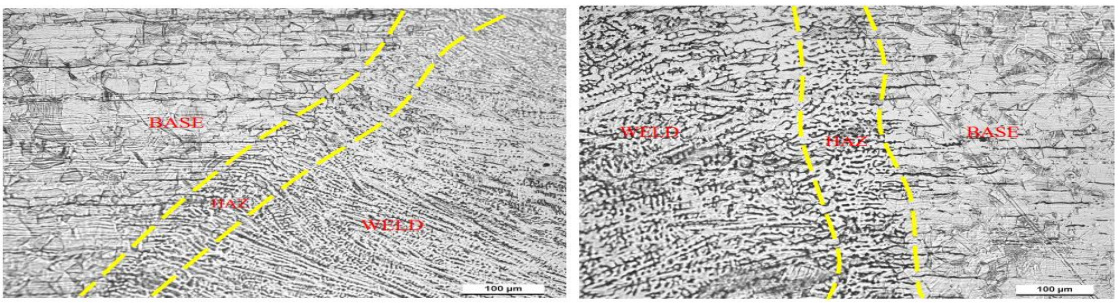

Figure 3.30 Metallographic view of sample number 9

All samples have pure austenitic grains with twin boundaries as far as the base metal's microstructure is concerned. Figure 3.21 depicts a microstructure of a base metal as an example.

The HAZ microstructures of nine samples show little variation. Microstructures of HAZs are generally found to be very similar to those of base metals. However, the grains of HAZ are found to be coarser than those of the base metals studied. The lower cooling rate in the HAZ region may be to blame for this. The above observation is supported by the results of a micro-hardness test. All samples have Austenitic twins in their HAZ. The presence of traces of -ferrite in HAZ can be seen in nearly all samples. Samples 3 and 9 both contain dispersed carbide phases in the HAZ region (Figure 3.24 and Figure3.30). The tensile strength of this sample is the lowest. A microstructural study of HAZ has found no significant cause for the high tensile test values of sample numbers 1, 2 and 7 (Figures 3.22, 3.23 and 3.28, respectively).

To compare the microstructures of weld metal and the microstructures of HAZ and base metal, it is found that weld metal microstructures look very different from the microstructures of these two materials. Weld microstructures show columner-dendritic grain growths in the majority of samples. However, in a few samples (samples 4 and 5; Figures 3.24 and 3.25) equi-axed grain growths can be seen in the weld metal.

The microstructures of various weldment zones have been influenced by parametric condition variation, but not in a straightforward way. However, the impact of changing welding parameters is undeniable. In the future, this may be taken into account more extensively.

3.7 TAGUCHI METHOD

Dr. Genichi Taguchi, a Japanese expert in quality management, came up with the Taguchi method. The Taguchi quality engineering methods, which use design of experiments, are an efficient and systematic way to optimise designs for performance, quality, and cost. For designing high-quality systems at a lower cost, it is an essential tool. Optically set process control parameters with Taguchi method, which is based on orthogonal array experiments, provides much reduced variance for the experiment results. There are less experiments in an orthogonal array, but the set of experiments is more well-balanced. Taguchi method uses a statistical measure of performance called signal-to-noise ratio to evaluate the optimal parameter setting, which takes into account both the mean and the variability. The method investigates the quadratic loss function concept. This ratio is the standard deviation divided by the mean (signal) (noise). The optimum ratio is determined by the product or process's quality characteristics. NB, LB, and HB are the three most commonly used standard signal-to-noise ratios (S/N ratios) (HB). The best S/N ratio is achieved by using the parametric combination. Multi-objective optimization cannot be solved using the traditional Taguchi method. You can accomplish this by using the Taguchi method based on grayscale images. There has been evidence to support Deng's grey system theory since it was first introduced in 1982. An effective method for resolving complex interrelationships among multiple performance characteristics is the grey relational analysis based on grey system theory. Experimental data, such as the quality characteristics of the product, are first normalised ranging from zero to one in order to perform grey relational analysis. Grey relational generation is the name given to this process. The grey relational coefficient is then calculated based on normalised experimental data to represent the correlation between the desired and actual data. The average of the grey relational coefficients for selected responses is then used to determine the overall grey relational grade. The calculated overall grey relational grade affects the multiple response process's overall performance characteristic. Optimizing a single response with the objective function can be done in the same way as optimising multiple responses in a process. It is then evaluated by maximising the S/N ratio of the overall grey relational grade, using a grey-Taguchi method.

Taguchi's S/N Ratio for (NB) Nominal-the-best

$$\eta = 10\ ln_{10}\frac{1}{n}\sum_{i=1}^{n}\frac{\mu^2}{\sigma^2} \tag{3.1}$$

Taguchi's S/N Ratio for (LB) Lower-the-better

$$\eta = -10\ ln_{10}\frac{1}{n}\sum_{i=1}^{n} y_i^2 \tag{3.2}$$

Taguchi's S/N Ratio for (HB) Higher-the-better

$$\eta = -10\ ln_{10}\frac{1}{n}\sum_{i=1}^{n}\frac{1}{y_i^2} \tag{3.3}$$

3.8 GREY RELATIONAL ANALYSIS

Experimental data, such as the quality characteristics of the product, are first normalised ranging from zero to one in order to perform grey relational analysis. Grey relational generation is the name given to this process. The grey relational coefficient is then calculated based on normalised experimental data to represent the correlation between the desired and actual data. The average of the grey relational coefficients for selected responses is used to determine the overall grey relational grade. The calculated grey relational grade has an impact on the multiple response process' overall performance characteristic. One of the main advantages of this method of solving multi-response optimization problems is that the overall objective function is graded in overall grey relational grades.. In order to determine the best parametric combination, the overall grey relational grade is used.

In grey relational generation, the normalized data corresponding to Lower-the-Better (LB) criterion can be expressed as:

$$x_i(k) = \frac{max\, y_i(k) - y_i(k)}{\max y_i(k) - min\, y_i(k)} \quad (3.4)$$

For Higher-the-Better (HB) criterion, the normalized data can be expressed as:

$$x_i(k) = \frac{y_i(k) - min\, y_i(k)}{max\, y_i(k) - min\, y_i(k)} \quad (3.5)$$

where $x_i(k)$ is the value after the grey relational generation, min $y_i(k)$ is the smallest value of $y_i(k)$ for the *kth* response, and max $y_i(k)$ is the largest value of $y_i(k)$ for the *kth* response. An ideal sequence x_0(k) is for the responses. The purpose of grey relational grade is to reveal the degrees of relation between the sequences says,[x_0(k) and x_i(k), i=1,2,3,…..,16]. The grey relation coefficient $\xi_i(k)$ can be calculated as

$$\xi_i(k) = \frac{\Delta_{min} + \theta \Delta_{max}}{\Delta_{0i}(k) + \theta \Delta_{max}} \quad (3.6)$$

Where $\Delta_{0i} = \| x_0(k) - x_i(k) \|$ difference of the absolute value x_0(k) and x_i(k); θ is the distinguishing coefficient $0 \leq \theta \leq 1$; $\Delta_{min} = \forall j^{min} \square\, i \forall k^{min} \| x_0(k) - xj(k) \| =$ the smallest value of Δ_{0i} ; and $\Delta_{max} = \forall j^{min} \square\, i \forall k^{min} \| x_0(k) - xj(k) \| =$ largest value of Δ_{0i}.

X_i and the comparative sequence X_0 (also called grey relational grade), and $\Delta_{0,i}(k)$ is the absolute value of difference between X_0 (k) and X_i (k).

After averaging the grey relation coefficients, the grey relational grade γ_i can be computed as:

$$y_i = \frac{1}{n} \sum_{k=1}^{n} \xi_i(k) \quad (3.7)$$

where n = number of process responses. The higher value of grey relational grade corresponds to intense relational degree between the reference sequence $x_0(k)$ and the given sequence $x_i(k)$. The reference sequence $x_0(k)$ represents the best process sequence. Therefore, higher grey relational grade means that the corresponding parameter combination is closer to the optimal.

3.9 OPTIMIZATION BY USING GREY-BASED TAGUCHI METHOD FOR L_9 TAGUCHI ORTHOGONAL ARRAY DESIGN OF EXPERIMENT

Responses (ultimate tensile strength and breaking tensile strength) of L_9 Taguchi orthogonal array design of experiment should be high, so normalizing the experimental data according to larger -the-better (LB) criterion by using the equation (3.5). Experimental data are collected as per L_9 Taguchi orthogonal array design matrix given discussed in chapter 2 and 3. Normalization of experimental data is shown in Table 3.5.

Table: 3.5 Normalization of experimental data based on L_9 Taguchi Orthogonal Array design of experiment.

Sample No.	*Yield Strength* (Mpa)	*Ultimate Tensile Strength* (Mpa)	*Percentage of Elongation*
Ideal sequence	1.0000	1.0000	1.0000
1	0.49273	0.97821	0.88793
2	0.00000	1.00000	1.00000
3	0.79645	0.00000	0.36207
4	0.49111	0.04720	0.05172
5	0.76898	0.06899	0.65517
6	0.65267	0.14742	0.63793
7	1.00000	0.76906	0.06897
8	0.65913	0.47131	0.15517

9	0.47819	0.01452	0.00000

Grey relation coefficients are shown in Table 3.6. Grey relation coefficient have been calculated by using equation 3.6

Table 3.6 Calculation of grey relational coefficients (ξi(k))

Sample No.	*Yield Strength* (Mpa)	*Ultimate Tensile Strength* (Mpa)	*Percentage of Elongation*
Ideal sequence	1.0000	1.0000	1.0000
1	0.50366	0.33825	0.36025
2	1.00000	0.33333	0.33333
3	0.38567	1.00000	0.58000
4	0.50448	0.91374	0.90625
5	0.39402	0.87875	0.43284
6	0.43378	0.77229	0.43939
7	0.33333	0.39399	0.87879
8	0.43136	0.51477	0.76316
9	0.51115	0.97177	1.00000

Grey relation grades for all performance characteristics have been calculated by using equation 3.7.

Overall grey relation grade of ultimate tensile strength and breaking tensile strength are shown in Table 3.7

Table 3.7 Calculation of overall grey relation grade

Sample No.	*Grey relation grade*
1	0.400719
2	0.555556
3	0.655223
4	0.774823
5	0.568534
6	0.548488
7	0.535371
8	0.569761
9	0.827640

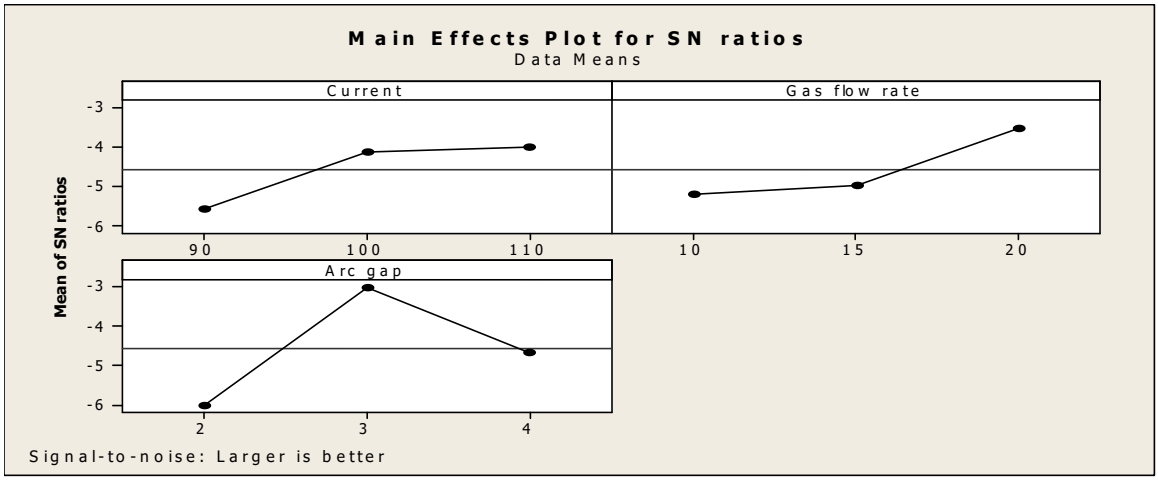

Figure 3.31 S/N ratio plot for overall grey relation grade

Mean values of overall grey relational grade is shown in Table 3.8

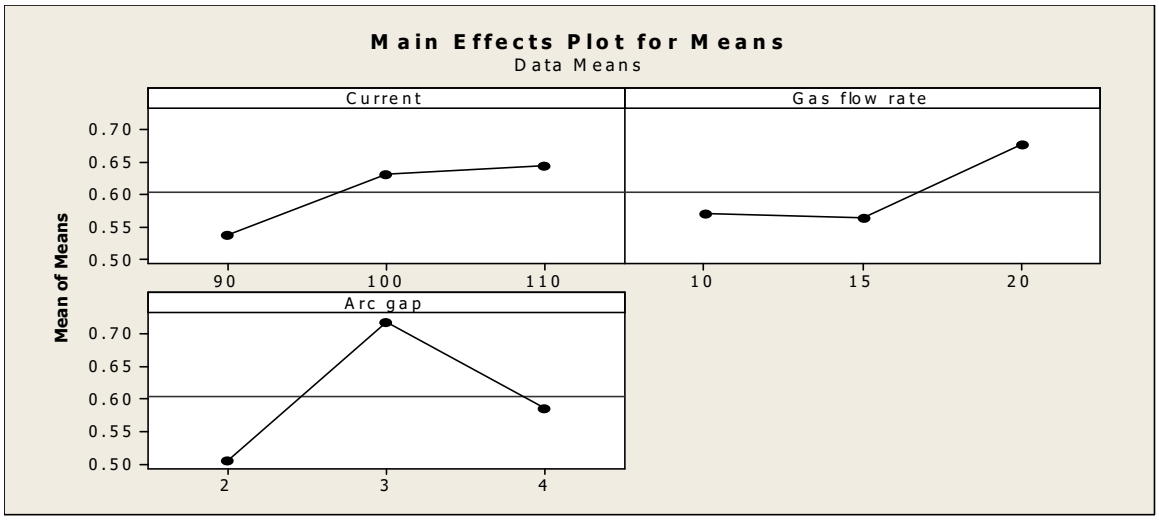

Figure 3.32 Main effect plot for means for overall grey relation grade

With the help of mean effect plots for S/N ratio and main effect plot for means (Figure 3.31 and Figure 3.32), optimum parametric combination has been determined. The optimal factor setting becomes **(C3G3A2)**

Table 3.8 Mean value table of overall grey relational grade

Level	Current	Gas flow rate	Arc Gap
1	0.5372	0.5703	0.5063
2	0.6306	0.5646	**0.7193**
3	**0.6443**	**0.6771**	0.5864
Delta	0.1071	0.1125	0.2130
Rank	3	2	1

Mean value of overall grey relational grade indicates the order of factors (ranking) representing the extent of significance on the overall grey relational grade.

Analysis of Variance for overall grey relational grade, using Adjusted SS for Tests is shown in Table 3.9

Table 3.9 Analysis of Variance for overall grey relational grade

SOURCE	DF	Seq SS	Adj SS	Adj MS	F	P	Significance	Percentage of contribution
Current	2	0.02039	0.02039	0.01019	0.94	0.516	significant	15.06
Gas flow rate	2	0.02410	0.02410	0.01205	1.11	0.475	significant	17.07
Arc Gap	2	0.06946	0.06946	0.03473	3.19	0.239	significant	51.19
Error	2	0.02176	0.02176	0.01088				16.03
Total	8	0.13571						

S = 16.6257 R-Sq = 98.58% R-Sq(adj) = 66.31%

RESULT OF CONFIRMATORY TEST:

Confirmatory tests have been done with respect to the analyses of L_9 Taguchi Orthogonal Array design of experiment. It is found that prediction of optimal parameter setting is valid. Tests have been organized and carried out in order to confirm the aforementioned optimal condition's validity. The findings are as follows: To illustrate that the proposed optimization process is working, the UTS at optimum state is 480.2 MPa.

CHAPTER 4

CONCLUSIONS AND FUTURE SCOPE OF WORK

4.1 CONCLUSIONS

Welding of Austenitic stainless steel by TIG: Based on the results of investigation and analyses, the following conclusions are made.

- Visual inspection and X-ray radiography test reveals that in few samples defects like porosity, lack of fusion, undercut occur. However, almost defect free joints are also observed, under some parametric conditions.
- Tensile test results are found to be satisfactory, excepting for few samples. The variations in input parameters have influenced the mechanical properties to a certain extent. Ultimate Tensile Strength (UTS) varies from 470 MPa to 590 MPa
- Measurement of hardness at different zones of weldment indicates that hardness in weld metal is more than hardness in HAZ and base metal. HAZ hardness is found to be a little bit smaller than base metal. However, variation in hardness at different zones is not found to be too excessive.
- Pure austenitic structure with significant amount of austenitic twin is found in the microstructure of base metal. No significant difference is observed in the microstructure of HAZ with respect to base metal microstructure. However, grain growth is observed in HAZ. Austenitic twins are also observed in HAZ and equiaxed grain is observed in weld metal. In some samples columnar dendritic growth is also found. Micro structural characteristics are more or less consistent with results of tensile test.
- Optimal condition is determined as Current 110A, Gas flow rate 20 l/min, Arc gap 3mm. This is the multi –objective optimization result, done by using Grey based Taguchi method for maximizing of UTS, YS and PE simultaneously
- Significance of each of the factors has been identified through ANOVA. Most significant factor is Welding current.

FUTURE SCOPE OF WORK

- In the present study, the welding parameters: current, gas flow rate and arc gap have been varied. The other parameters like voltage, welding speed, filler rod diameter could also be taken into account. This provides the scope of future work.

- Experiments may be planned for TIG welding of some other types of austenitic stainless steel (i.e other than 304 types).

- The data of the present work (if needed with more number of experiment runs) may be used to build up a reliable Artificial Neural Network model for prediction of the responses under given set of input parameters.

- In the present study, 3 mm thickness of austenitic stainless steel has been used. The study may be extended to some other thickness (both smaller and larger) of the material.

- Effect of process parameters with variation in edge preparation may also be studied in respect of TIG welding of stainless steel.

- Study of weld micro structures has been taken up to limited extent in the present work. Obviously, the effect of process parameters on the microstructures of the weldment is an important area to be investigated in future more extensively for TIG welding of austenitic stainless steel.

- Determination of HAZ width, hardness of different zones of the weldment, weld-metal chemistry etc. provide plenty scope of future work.

- Analysis of the data and optimization of the process parameters may be carried out using several standard and newer techniques and the usefulness of each technique may be evaluated.

REFERENCES

[1] Q.Wang, D.L.Sun, Y.Na, Y.Zhou, X.L.Han˙J. Wang. "*Effects of TIG Welding Parameters on Morphology and Mechanical Properties of Welded Joint of Ni-base Superalloy*", Procedia Engineering 10 (2011) 37–41.

[2] Izzatul Aini Ibrahim , Syarul Asraf Mohamat , Amalina Amir , Abdul Ghalib, "*The Effect of Gas Metal Arc Welding (GMAW) processes on different welding parameters*", Procedia Engineering 41 (2012) 1502 – 1506.

[3] Indira Rani M , R N Marpu, "*Effect of Pulsed Current Tig Welding Parameters on Mechanical Properties of J-Joint Strength of Aa6351*", The International Journal of Engineering And Science (IJES), Volume, 1, Issue, 1, Pages: 01-05, Nov 2012, ISSN: 2319–1813 ISBN: 2319–1805.

[4] Erdal Karadeniz , Ugur Ozsarac, Ceyhan Yildiz, "*The effect of process parameters on penetration in gas metal arc welding processes*", Materials and Design 28 (2007) 649–656.

[5] S. P. Tewari, Ankur Gupta, Jyoti Prakash, "*Effect of Welding Parameters on the Weldability of Material*", International Journal of Engineering Science and Technology Vol. 2(4), 2010, 512-516, ISSN: 0975-5462.

[6] N.Jeyaprakash, Adisu Haile, M. Arunprasath, "*The Parameters and Equipments Used in TIG Welding: A Review*", The International Journal Of Engineering And Science (IJES), Volume, 4 Issue, 2, Pages: PP.11-20, 2015, ISSN (e): 2319 – 1813 ISSN (p): 2319 – 1805.

[7] K. Kishore, P. V. Gopal Krishna, K. Veladri and Syed Qasim Ali, "*Analysis of Defects in Gas Shielded Arc Welding of AISI1040 Steel Using Taguchi Method*", ARPN Journal of Engineering and Applied Sciences, VOL. 5, NO. 1, JANUARY 2010 ISSN 1819-6608, Page-37-41.

[8] S. R. Patil, C. A. Waghmare, "*Optimization of MIG Welding Parameters for Improving Strength of Welded Joints*", International journal of Advanced Engineering Research and Studies E-ISSN2249-8974, Int. J. Adv. Engg. Res. Studies /II/IV/ July-Sept., 2013/14-16

[9] Farhad Kolahan, Mehdi Heidari, "*A New Approach for Predicting and Optimizing Weld Bead Geometry in GMAW*", International Journal of Mechanical Systems Science and Engineering 2:2 2010, Pages- 138-142.

[10] Satya dutt sinha P. Chavda , Jayesh V.Desai , Tushar M. Patel, "*A Review on Optimization of MIG Welding Parameters using Taguchi's DOE Method*", International Journal of Engineering and Management Research Available at: www.ijemr.net Page Number: 16-21, Volume-4, Issue-1, February-2014, ISSN No.: 2250-0758

[11] Jose L Meseguer-Valdenebro, Antonio Portoles, J Onoro, "*Numerical study of TTP curves upon welding of 6063-T5 aluminum alloy and optimization of welding process parameters by Taguchi's method*", Indian Journal of Engineering & Materials Science, Vol. 23, Octobor 2016, pp.341-348.

[12] Diganta Kalita, Parimal Bakul Barua, "*Taguchi Optimization of MIG Welding Parameters Affecting Tensile Strength of C20 Welds*", International Journal of Engineering Trends and Technology (IJETT) – Volume 26 Number 1- August 2015, ISSN: 2231-5381, http://www.ijettjournal.org/ , PageNumber: 43 -49.

[13] Chandresh. N. Patel, Sandip Chaudhary, "*Parametric Optimization of Weld Strength of Metal Inert Gas Welding and Tungsten Inert Gas Welding By Using Analysis of Variance and Grey Relational Analysis*", International Journal of Research in Modern Engineering and Emerging Technology, Vol. 1, Issue: 3, April-2013 (IJRMEET) ISSN: 2320-6586, Pages- 48-56.

[14] S. D. Ambekar, Sunil R.Wadhokar, "*Parametric Optimization of Gas metal arc welding process by using Taguchi method on stainless steel AISI 410*", International Journal of Research in Modern Engineering and Emerging Technology, Vol. 3, Issue: 1, January : 2015 (IJRMEET) ISSN: 2320-6586, Pages- 1-9.

[15] Neha Agrawal, Meenakshi Thakur, Janmit Raj, Anand Baghel, "*A Review on TIG/MIG Welded Joints*", IJSTE - International Journal of Science Technology & Engineering, Volume 4, Issue 1, July 2017 ISSN (online): 2349-784X, http://www.ijste.org/ , Page Number: 65-71

[16] Kumar Rahul and Vijay Mittal, "Review on the parametric optimization of TIG welding", International Research Journal of Engineering and Technology (IRJET), Volume: 04 Issue: 01 | Jan -2017, e-ISSN: 2395 -0056, p-ISSN: 2395-0072, http://www.irjet.net/, Pages- 1266-1268.

[17] Saadat Ali Rizvi, S.P Tewari, "*Optimization of Welding Parameters by Using Taguchi Method and Study of Fracture Mode Characterization of SS304H Welded by GMA Welding*", Jordan Journal of Mechanical and Industrial Engineering, Volume 12 Number 1, June. 2018 ISSN 1995-6665 Pages 17 – 22

[18] C Prabaharan, P Venkatachalam, K Suresh, K Lenin,"*Parametric Optimization of Gas Tungsten Arc Welding Process by Using Factorial Design Approach*", Journal of Science Industrial Research Vol 73, June 2014, pp. 415-420

[19] Omar Bataineh, Al-Shoubaki, Omar Barqaw, "*Optimising Process Conditions in MIG Welding of Aluminum Alloys Through Factorial Design Experiments*", Latest Trends in Environmental and Manufacturing Engineering, ISBN: 978-1-61804-135-7, Pages- 21-26.

[20] Mohan B. Raut, S. N. Shelke, "*Optimization of Special Purpose Rotational MIG Welding by Experimental and Taguchi Technique*", International Journal of Innovative Technology and Exploring Engineering (IJITEE) ISSN: 2278-3075, Volume-4 Issue-6, November 2014, Pages- 39-46.

[21] Shekhar Srivastava, R.K. Garg, "*Process parameter optimization of gas metal arc welding on IS: 2062 mild steel using response surface methodology*", Journal of Manufacturing Processes 25 (2017) 296–305

[22] Stephen A. Akinlabi and Madindwa P. Mashinini, Cynthia S. Abima, Olawale S. Fatoba and Esther T. Akinlabi, "*TIG & MIG Hybrid Welded Steel Joint: A Review*", Proceedings of the International Conference on Industrial Engineering and Operations Management Toronto, Canada, October 23-25, 2019, Page No: 801-811.

[23] Cynthia Samuel Abimaa et al. "*Multi-Objective Optimization of process parameters in TIG-MIG welded AISI 1008 steel for improved structural integrity*", The International Journal of Advanced Manufacturing Technology (2022) 118:3601–3615, https://doi.org/10.1007/s00170-021-08181-1,

[24] P. Vasantharaja, M. Vasudevana, P. Palanichamy, "*Effect of welding processes on the residual stress and distortion in type 316LN stainless steel weld joints*", Journal of Manufacturing Processes 19 (2015) 187–193.

[25] V. Anand Rao and R. Deivanathan , "*Experimental Investigation for Welding Aspects of Stainless Steel 310 for the Process of TIG Welding*", Procedia Engineering 97 (2014) 902 – 908

[26] M. Anuradha et al. "*Effect of Welding Parameters on TIG Welding of Inconel 718 to AISI 4140 Steel*", Trans Indian Inst Met (2020) 73(6):1515–1520

[27] A.F. Norman, V. Drazhner, P.B. Prangnell. "*Effect of welding parameters on the solidification microstructure of autogenous TIG welds in an Al–Cu–Mg–Mn alloy*", Materials Science and Engineering A259 (1999) 53–64

[28] L. Natrayan, R. Anand, S. Santhosh Kumar, "*Optimization of process parameters in TIG welding of AISI 4140 stainless steel using Taguchi technique*", Materials Today: Proceedings, https://doi.org/10.1016/j.matpr.2020.07.150, Pages- 1-4.

[29] Paulo J. Modenesi et al. "*TIG welding with single-component fluxes*", Journal of Materials Processing Technology 99 (2000) 260-265

[30] Akash. B. Patel, Satyam. P. Patel, "*The effect of activating fluxes in TIG welding by using Anova for SS 321*", Int. Journal of Engineering Research and Applications www.ijera.com ISSN : 2248-9622, Vol. 4, Issue 5(Version 5), May 2014, pp.41-48

[31] Ahmed Khalid Hussain et al. "*Influence of Welding Speed on Tensile Strength of Welded Joint in TIG Welding Process*", InternationalJournal of Applied Engineering Research, Din Digul Volume 1, No 3, 2010,ISSN - 0976-4259, Pages- 518-527

[32] J. Pasupathy and V. Ravisankar, "*Parametric optimization of TIG welding parameters using Taguchi method for dissimilar joint*", International Journal of Scientific & Engineering Research, Volume 4, Issue 11, november-2013 ISSN 2229-5518, Pages- 25-28

[33] Asif Ahmad, ShahnawajAlam, "*Parametric optimization of TIG welding using Response Surface Methodology*", Materials Today: Proceedings 18 (2019) 3071–3079

[34] Arun Kumar Srirangan, Sathiya Paulraj, "*Multi-response optimization of process parameters for TIG welding of Incoloy 800HT by Taguchi grey relational analysis*", Engineering Science and Technology, an International Journal http://dx.doi.org/10.1016/j.jestch.2015.10.003,

[35]Ugur Esme, Melih Bayramoglu, Yugut Kazancoglu, Sueda Ozgun, " *Optimization of weld bead geometry in TIG welding process using Grey relation analysis and Taguchi method*", Materials and technology 43 (2009) 3, 143–149, ISSN 1580-2949 Original scientific article MTAEC9, 43(3)143(2009), UDK 621.791.05

[36] Jay J. Vora, Kumar Abhishek, Seshasai Srinivasan, "*Attaining optimized A-TIG welding parameters for carbon steels by advanced parameter-less optimization techniques:*

with experimental validation", Journal of the Brazilian Society of Mechanical Sciences and Engineering (2019) 41:261 https://doi.org/10.1007/s40430-019-1765-0

[37] Vishal Chaudhari et al. "*Parametric optimization of TIG welding on SS304 and MS using Taguchi approach*", International Research Journal of Engineering and Technology (IRJET) e-ISSN: 2395-0056, p-ISSN: 2395-0072, Volume: 06 Issue: 05 | Apr 2019, page no.-880-885.

[38]G. Sathish Kumar et al. "*Investigation of the TIGWelding Process for Joining AA6082 Alloy Using Grey Relational Analysis*", Hindawi Advances in Materials Science and Engineering Volume 2022, Article ID 5670172, 8 pages, https://doi.org/10.1155/2022/5670172,

[39]Sriramoju Avinash et al. "*Multi-response optimization of pulse TIG welding process parameters of welds AISI 304 and Monel 400 using grey relational analysis*", Materials Today: Proceedings, https://doi.org/10.1016/j.matpr.2019.07.211.

[40] Balram Yelamasetti et al. "*Multi-response Taguchi grey relational analysis of mechanical properties and weld bead dimensions of dissimilar joint of AA6082 and AA7075*", advances in materials and processing technologies, https://doi.org/10.1080/2374068X.2021.1946340,

[41] K. Mahendra Babu et al.," *Optimization of Process Parameters Affecting TIG Welding of AA 6082 by Grey Relational Analysis*", International Journal of Engineering Research & Technology (IJERT) http://www.ijert.org ISSN: 2278-0181 IJERTV7IS050042 Published by : www.ijert.org Vol. 7 Issue 05, May-2018, page no: 39-41

[42] V. Vinoth, et al. "Optimization of mechanical behaviour of TIG welded 316 stainless steel using Taguchi based grey relational analysis method", Materials Today: Proceedings, https://doi.org/10.1016/j.matpr.2020.12.1002.

[43] M. Vasudevan et al. "*Genetic algorithm for optimisation of A-TIG welding process for modified 9Cr–1Mo steel*", Science and Technology of Welding and Joining, 2010 VOL 15 NO 2, page no: 117-123.

[44]Joby Joseph, S. Muthukumaran, "*Optimization of activated TIG welding parameters for improving weld joint strength of AISI 4135 PM steel by genetic algorithm and simulated annealing*", Int J AdvManufTechnol (2017) 93:23–34 DOI 10.1007/s00170-015-7599-8, page no: 23-34

[45] L. Srinivasan et al. "*Application of Genetic Algorithm Optimization Technique in TIG Welding of 15CDV6 Aerospace Steel*", Silicon (2019) 11:459–469, https://doi.org/10.1007/s12633-018-9862-8, page no: 459-469.

[46] S. Mondal, G. Nandi, P. K. Pal,"*Parametric optimization of TIG welding of duplex stainless steel without filler rod by PCA method*", IOP Conf. Series: Materials Science and Engineering 1017 (2021) 012007 IOP Publishing doi:10.1088/1757-899X/1017/1/012007.

[47] J. Mirapeix, et al., "*Real-time arc-welding defect detection and classification with principal component analysis and artificial neural networks*", NDT&E International 40 (2007) 315–323.

[48] Prashant S Lugade , Manish J Deshmukh, "*Optimization of Process Parameters of Activated Tungsten Inert Gas (A-TIG) Welding for Stainless Steel 304L using Taguchi Method*", International Journal of Engineering Research and General Science Volume 3, Issue 3, May-June, 2015 ISSN 2091-2730, page no: 854-860.

[49] S. Omprakasam, et al. "*Statistical Modelling and Optimization of TIG Welding Process Parameters Using Taguchi's Method*", Strojniškivestnik - Journal of Mechanical Engineering 68(2022)3, 200-209.

[50] E. Ahmadi, A.R. Ebrahimi , "*The effect of activating fluxes on 316L stainless steel weld joint characteristic in TIG welding using the Taguchi method* ",Journal of Advanced Materials and Processing, Vol. 1, No. 1, 2012, 55-62.

[51] Mohamed Farid Benlamnouar et al. "*Optimization of TIG Welding Process Parameters for X70-304L Dissimilar Joint Using Taguchi Method*", Industrial Processes of Multi-Material Assembly, Solid State Phenomena Vol. 297, ISSN: 1662-9779, Vol. 297, pp 51-61, https://doi.org/10.4028/www.scientific.net/SSP.297.51.

[52] D.S. Nagesha, G.L. Datta, "*Genetic algorithm for optimization of welding variables for height to width ratio and application of ANN for prediction of bead geometry for TIG welding process*", Applied Soft Computing 10 (2010) 897–907.

[53] Shamith L Saldanha, V Kalaichelvi, R Karthikeyan, "*Prediction Analysis of Weld-Bead and Heat Affected Zone in TIG welding using Artificial Neural Networks*", IOP Conf. Series: Materials Science and Engineering 346 (2018) 012038 doi:10.1088/1757-899X/346/1/012038.

[54] Daniel Bacioiua et al., "*Automated defect classification of Aluminium 5083 TIG welding using HDR camera and neural networks*", Journal of Manufacturing Processes, https://doi.org/10.1016/j.jmapro.2019.07.020, page no: 603-613.

[55] I. Owunna, A. E.Ikpe,"*Modeling and prediction of the mechanical properties of YIG welding joint for AISI 4130 low carbon steel plates using Artificial Neural Network (ANN) approach*", Nigerian Journal of Technology (NIJOTECH) Vol. 38, No. 1, January 2019, pp. 117 – 126, http://dx.doi.org/10.4314/njt.v38i1.1.

[56] Rohit Kshirsagar et al. "*Prediction of Bead Geometry Using a Two-Stage SVM–ANN Algorithm for Automated Tungsten Inert Gas (TIG) Welds*", J. Manuf. Mater. Process. 2019, 3, 39, http://www.mdpi.com/journal/jmmp.

[57] Ghosh, A.; Mallik, A. K. *Manufacturing Science;* Ellis Horwood Ltd, Publisher: Harlow, England, 1986.

[58] RAO. *Manufacturing Technology: Foundry, Forming and Welding,* 2nd ed.; McGraw-HillEducation: London, England, 1999.

[59] https://marinegyaan.com/what-are-defects-or-faults-of-welding/

[60] https://weldguru.com/tig-equipment/